JGR Oceans

Key Points:

- Dissolved Organic Matter (DOM) distribution in the Arctic Ocean is largely controlled by sea ice formation and melt processes
- DOM distribution in the Arctic Ocean reveals its potential as a tracer for halocline formation and freshwater source assignments
- Terrigenous and marine DOM are carriers of trace elements from shelves to the open Arctic Ocean, but terrigenous DOM represent stronger ligands

Spatial Complexity in Dissolved Organic Matter and Trace Elements Driven by Hydrography and Freshwater Input Across the Arctic Ocean During 2015 Arctic GEOTRACES Expeditions

Tatiana Williford[1] , Rainer M. W. Amon[1,2] , Karl Kaiser[1,2] , Ronald Benner[3] , Colin Stedmon[4] , Dorothea Bauch[5,6] , Jessica N. Fitzsimmons[1] , Loes J. A. Gerringa[7] , Robert Newton[8] , Dennis A. Hansell[9] , Mats A. Granskog[10] , Laramie Jensen[1] , Luis M. Laglera[11] , Angelica Pasqualini[8], Benjamin Rabe[12] , Heather Reader[13] , Michiel Rutgers van der Loeff[12] , and Ge Yan[2]

[1]Texas A&M University, Galveston, TX, USA, [2]Texas A&M University Galveston Campus, Galveston, TX, USA, [3]University of South Carolina, Columbia, SC, USA, [4]Technical University of Denmark, Kongens Lyngby, Denmark, [5]Leibniz-Laboratory, University of Kiel CAU, Kiel, Germany, [6]GEOMAR Helmholtz Centre for Ocean Research, Kiel, Germany, [7]Royal Netherlands Institute for Sea Research, Den Hoorn, The Netherlands, [8]Columbia University, New York, NY, USA, [9]Rosenstiel School of Marine and Atmospheric Sciences, Miami, FL, USA, [10]Norwegian Polar Institute, Fram Centre, Tromsø, Norway, [11]Universidad de las Islas Baleares, Palma, Spain, [12]Alfred-Wegener Institute for Polar- und Marine Research, Bremerhaven, Germany, [13]Memorial University of Newfoundland, St. John's, NL, Canada

Abstract This study traces dissolved organic matter (DOM) in different water masses of the Arctic Ocean and its effect on the distributions of trace elements (TEs; Fe, Cu, Mn, Ni, Zn, Cd) using fluorescent properties of DOM and the terrigenous biomarker lignin. The Nansen, Amundsen, and Makarov Basins were characterized by the influence of Atlantic water and the fluvial discharge of the Siberian Rivers with high concentrations of terrigenous DOM (tDOM). The Canada Basin and the Chukchi Sea were characterized by Pacific water, modified through contact with productive shelf sediments with elevated levels of marine DOM. Within the surface layer of the Beaufort Gyre, meteoric water (river water and precipitation) was characterized by low concentrations of lignin and tDOM fluorescence proxies as DOM is removed during freezing. High-resolution in situ fluorescence profiles revealed that DOM distribution closely followed isopycnals, indicating the strong influence of sea-ice formation and melt, which was also reflected in strong correlations between DOM fluorescence and brine contributions. The relationship of DOM and hydrography to TEs showed that terrigenous and marine DOM were likely carriers of dissolved Fe, Ni, Cu from the Eurasian shelves into the central Arctic Ocean. Chukchi shelf sediments were important sources of dCd, dZn, and dNi, as well as marine ligands that bind and carry these TEs offshore within the upper halocline in the Canada Basin. Our data suggest that tDOM components represent stronger ligands relative to marine DOM components, potentially facilitating the long-range transport of TE to the North Atlantic.

Plain Language Summary The Arctic Ocean receives a disproportionate large amount of global river discharge and has limited but well-constrained exchanges with other oceans. This makes the Arctic Ocean unique in terms of dissolved organic matter (DOM) and trace element (TE) sources and distribution. We used data collected during two expeditions spanning the entire Arctic Ocean to characterize the unique distribution of DOM and to study its potential as a water mass tracer and its role in the transport of TE. While the Atlantic-dominated Nansen Basin was characterized by low levels of the DOM and TE, the central Arctic was dominated by the Transpolar Drift, a current that connects the Eurasian shelves to the Fram Strait and transports DOM from the Siberian Rivers toward the North Atlantic. In contrast, the Chukchi shelf-Canada Basin region was characterized by the dominance of Pacific water that is enriched by marine DOM from the shallow and productive Chukchi shelf. The distribution of DOM from these different sources was affected by freezing and thawing processes and, therefore, can be used to study water mass transformations and pathways in the Arctic Ocean.

1. Introduction

Shifts in circulation regimes (Proshutinsky & Johnson, 1997), changes in the freshwater budget due to sea ice decline (Li et al., 2021), and increasing fluvial discharge (Ahmed et al., 2020; Fichot et al., 2013) in the Arctic Ocean are believed to influence the strength of the Atlantic Meridional Overturning Circulation and can have global impacts (Bruhwiler et al., 2021; Jiang et al., 2021; Zhang et al., 2021). State-of-the-art climate models (e.g., Jiang et al., 2021; Proshutinsky et al., 2020), remote sensing (e.g., Fichot et al., 2013), and observations (e.g., Guay et al., 2009; Polyakov et al., 2013; Rabe et al., 2014; Yamamoto-Kawai et al., 2009) have focused on the freshwater balance in the Arctic Ocean. In particular, studies have concentrated on the expanding Beaufort Gyre, an anticyclonic system in the Canada Basin that maintains the largest oceanic freshwater reservoir in the Arctic Ocean (Proshutinsky et al., 2019). Freshwater sources include fluvial discharge, Pacific water (which is less saline than Atlantic water), net precipitation, and sea ice melt (Carmack et al., 2008; Haine et al., 2015; Proshutinsky et al., 2019; Yamamoto-Kawaii et al., 2008). Environmental variability is imprinted in the chemical and optical properties of the omnipresent DOM, which makes dissolved organic matter (DOM) a tracer of freshwater sources as well as mixing processes in the ocean.

For example, we use lignin phenols, unique biomarkers of terrigenous DOM (tDOM) in the ocean (Benner et al., 2005; Kaiser et al., 2017; Opsahl & Benner, 1997; Opsahl et al., 1999; Williford et al., 2021), as a tracer of fluvial DOM in the Arctic Ocean. In addition to this terrigenous biomarker (lignin), we use the optical properties of chromophoric DOM (CDOM), including Parallel Factor Analysis (PARAFAC) of fluorescent DOM (Gonçalves-Araujo et al., 2016; Stedmon et al., 2021). Besides the characterization of surface waters of the Arctic Ocean, we are interested in the halocline layers with respect to DOM. In particular, we are interested how DOM can inform about the sources, distribution, and generation mechanisms of Arctic halocline layers and how that affects TE transport.

The Arctic Ocean is an ideal place to study metal-DOM interactions because it has limited exchanges with other oceans and has abundant sources of DOM and trace elements (TEs) in the upper water column, including fluvial discharge and input from productive shelf regions. Arctic rivers are an important source of both DOM and dissolved trace metals on the shelves and in the central basins of the Arctic Ocean (Amon, 2004; Amon et al., 2012; Benner, 2011; Benner et al., 2005; Charette et al., 2020; Jensen et al., 2020; Klunder et al., 2012; Krachler et al., 2012; Opsahl et al., 1999; Williford et al., 2021). Climate change-induced permafrost thaw, tundra greening, and coastal erosion enhance the mobilization of carbon from terrestrial Arctic ecosystems (Berner et al., 2020; Fritz et al., 2017), with a cascading effect on the supply of tDOM and TEs (Berner et al., 2020; Pokrovsky et al., 2012). Poor understanding of the complex relationships among organic ligands and dissolved trace metals in seawater has limited our ability to predict the magnitude of certain metal fluxes, the spatial extent of their transport away from their source, and the rate of metal scavenging and biological uptake to the particulate phase across a range of metals. In addition to the geochemical and biological factors, other factors like the electron configuration of a trace metal also affect ligand preference through the spatial arrangement of binding sites. For example, iron-ligand associations can range from monodentate to hexadentate complexation (Butler & Theisen, 2010; Williford et al., 2021). Molecular size also impacts the binding strength of ligands, with higher-molecular-weight molecules typically having a greater number of binding sites, more flexible molecular geometries, and greater binding strength (Laglera & van den Berg, 2009; Williford et al., 2021).

In this study, we explore the potential of DOM as a tracer of river discharge, freezing/thawing processes, and water mass pathways using biomarker lignin and examining the optical properties of CDOM. We characterize prominent Arctic features like the Beaufort Gyre, Transpolar Drift (TPD), upper and lower haloclines (UHC, LHC) in terms of DOM concentration and origin. Additionally, we examine potential links between hydrography, diverse groups of DOM molecules and several dissolved trace metals (dFe, dMn, dNi, dCu, dZn, dCd) across the breadth of the Arctic Ocean.

2. Materials and Methods

2.1. Hydrographic Context

Discrete water samples, in situ CDOM fluorescence, and hydrographic data were collected in the summer of 2015 during the U.S. Arctic GEOTRACES (GN01) cruise aboard the USCGC *Healy* (HLY1502) and the GEOTRACES TransARC II cruise (PS94) on the German research icebreaker *Polarstern* (Figure 1; Rabe et al., 2016a, 2016b;
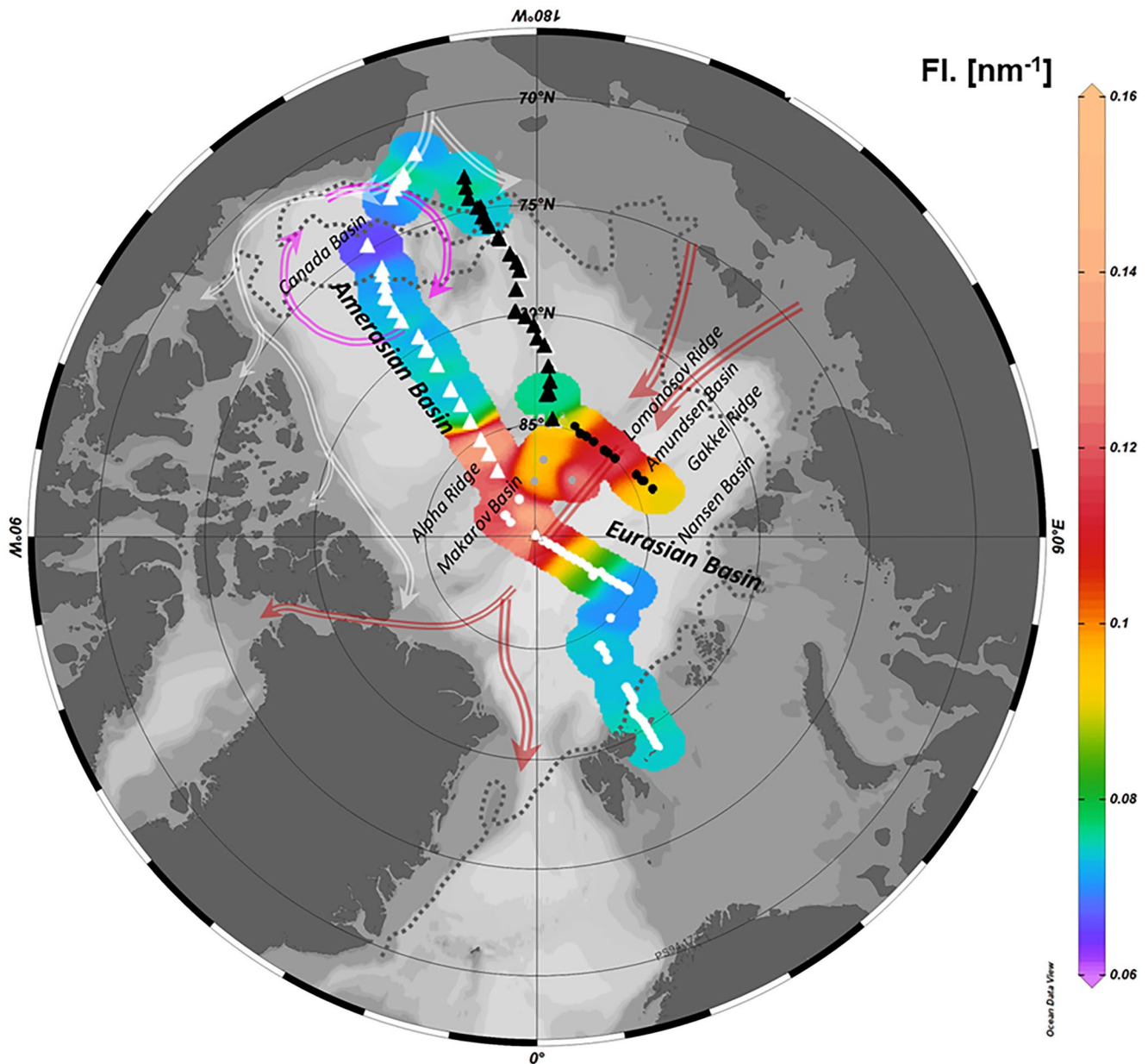
Figure 1. The U.S. GEOTRACES Arctic GN01 transect cruise track (triangles) and the TransARCII PS94 cruise track (squares). The approximate locations of major upper ocean circulation features are shown in gray, red (Transpolar Drift), and magenta (Beaufort Gyre). Surface in situ chromophoric DOM (CDOM) fluorescence (Fl.) in surface waters is shown in color (in nm^{-1}), extrapolated out to 100 km for visualization purposes. The gray dotted line indicates the sea ice edge at the time of sampling (August 2015, NSIDC database, 2015). Section A is shown in white symbols; Section B is shown in black symbols. In situ CDOM fluorescence was not measured along most of the Amerasian Basin portion of Section B. This figure and section plots in the manuscript were generated using Ocean Data View (Schlitzer, 2020).

Schauer, 2016). The GN01 cruise track (9th August–12th October 2015; Kadko & Landing, 2015) consisted of a "northbound" transect along ~170°–180°W stretching through Bering Strait and across the Canada and Makarov Basins to the North Pole (GN01 stations 1–32), and the "southbound" transect returning southward along ~150°W across the Makarov and Canada Basins back into Chukchi shelf waters (GN01 stations 33–57). The PS94 cruise track (17th August–15th October; Schauer, 2016) consisted of two transects extending from the Barents Sea and the Gakkel Ridge, respectively, into the Makarov Basin. The CTD data can be found at the PANGAEA data archive (https://www.pangaea.de: https://doi.org/10.1594/PANGAEA.859558), the British

Oceanographic Data Center (http://www.bodc.ac.uk/geotraces), and Biological and Chemical Oceanography Data Management Office (Landing et al., 2017, 2019).

The U.S. GEOTRACES GN01 and the TransARCII PS94 missions included two inter-calibration stations. Data from the North Pole station were collected synchronously (PS94 station 87, corresponding to GN01 station 32), while those from the deep Makarov Basin at 87°30'N 180°E (PS94 station 101, corresponding to GN01 station 30) were collected two weeks apart.

Here we define Section A (white symbols, Figure 1) as stretching from the Chukchi Sea shelf, across the North Pole (GN01 stations), and through the Amundsen and Nansen Basins to the Barents Sea (PS94 stations). The following hydrographic distinctions of water masses were assigned. The thickness of the relatively fresh polar mixed layer (PML, $S < 31$) is conventionally defined by the temperature minimum (Rudels et al., 1996). However, in cases where the temperature minimum cannot be identified with certainty, the rapid change in magnitude of the salinity gradient may be used (Korhonen et al., 2013). For example, the Chukchi Sea and southern Canada Basin are strongly influenced by seasonal sea ice melt, resulting in a near-surface temperature maximum from radiative warming of surface waters during summer (Jackson et al., 2010; Shimada et al., 2001). The average depth of winter convection is about 45 m in the northern Canada Basin and 35 m in the southern Canada Basin (Korhonen et al., 2013). In the Amundsen and Makarov basins, the PML deepens to about 55 m, becomes shallower, and occupies a depth of 40–50 m in the Nansen Basin (Korhonen et al., 2013; Rudels, 2009).

In the Canada Basin, underneath PML lies the upper halocline (UHC), in the Canada Basin largely derived from Pacific water. Because of its origin, the boundary between the upper and the LHCs is roughly defined by the isohaline of $S = 34$ (Korhonen et al., 2013). The Beaufort Gyre is a large anticyclonic system in the surface layer of the Canada Basin, marked by low salinity and low in situ CDOM fluorescence (Figure 1). Shelf-waters within the UHC and LHC are pushed downward by convergence associated with Ekman forcing in the surface Beaufort Gyre (Watanabe, 2013). According to climatology (Korhonen et al., 2013), the UHC is the thickest (180–200 m) in the southern Canada Basin. In the Makarov and Amundsen Basins, the thickness decreases to 40 and 30 m, respectively, and in the Nansen Basin, the UHC is generally absent (Korhonen et al., 2013). The LHC thickness in the Canada Basin varies between 60 and 70 m and increases toward the central Arctic Basins (~80 m in the Amundsen and Makarov Basins) and becomes thinner, <50 m, in the Nansen Basin (Korhonen et al., 2013). The Atlantic Water (AW; $S > 34.7$; Rudels, 2001) beneath the haloclines transitions into dense ($\sigma > 28$ kg/m^3) deep water below 1,000 m depth.

Section B (black symbols, Figure 1) is closer to the Eurasian slope and consists of the "northbound" leg of the GN01 cruise and the PS94 cruise transect between stations 117 and 134. Unfortunately, in situ CDOM fluorescence was not measured along most of the Amerasian Basin portion of Section B (Figure 1). Like Section A, Section B crossed the Amundsen and Makarov Basins, where the TPD can be observed by elevated surface in situ CDOM fluorescence.

2.2. Optical Properties of DOM

Water samples collected for absorption and fluorescence analyses were filtered through a 0.2 μm Millipore filter cartridge attached to Niskin bottles mounted on a CTD rosette. CDOM fluorescence was measured by two independent approaches. An in situ approach using backscatter fluorescence sensors with a broadband excitation of 350–460 nm and 550 ± 20 nm emission. The two instruments used on the ships were intercalibrated using the method introduced and discussed in Stedmon et al. (2021). The fluorescence intensities at excitation 350 and emission 450 nm measured in the water samples collected onboard at the same time were used to calibrate the voltage signal from the CTD-mounted Dr. Haardt fluorometers.

The second approach to determine CDOM fluorescence was a laboratory measurement of collected water samples using a bench-top spectrofluorometer. For the PS94 portion of the samples, Horiba Aqualog spectrofluorometer was used, and the details for the fluorescence measurements are described in Stedmon et al. (2021). For the GN01 portion, 132 samples were collected for DOM fluorescence measured using a Photon Technologies International spectrofluorometer (Quanta Master-4 SE) with a 1 cm quartz cuvette. Excitation-emission matrix scans (EEMs) for each sample covering emission from 280 to 600 nm (2 nm increment) and excitation wavelengths ranging from 220 to 450 nm (5 nm increment). Daily pure water (Milli-Q®) blanks were obtained and subtracted to remove water scattering peaks. Data were spectrally corrected for instrument bias, and subsequently, Raman calibrated

(excitation 350 nm) using the pure water blanks and the drEEM toolbox (version 0.2.0, Murphy et al., 2013). The Dr. Haardt signal was linearly correlated to the excitation 350 nm and emission 450 nm signal measured by the laboratory spectrofluorometer (Figure S1 in Supporting Information S1) to correct for the offset between the two sensors as described in Stedmon et al. (2021).

Studies show that not all of the instrument bias is removed using the manufacturer's spectral correction procedures (Cory et al., 2010). This problem is particularly important when multivariate data analyses will be applied. To circumnavigate the potential minor spectral differences, the datasets collected using different instruments were analyzed separately. Excitation below 250 nm was not included due to excessive instrument noise resulting from poor lamp output.

Two PARAFAC models were developed for the EEMs data: a four-component model was developed for the GN01 data set (C1) and a six-component model for the PS94 data set (C2). The four-component model (C1) was optimized based on spectral loadings, residual examination, and split-half validation using a convergence criterion of $1e^{-8}$ (Figure S2a in Supporting Information S1). The components were labeled based on their emission maxima: $C1_{482}$, $C1_{428}$, $C1_{402}$, $C1_{348}$. For the EEMs from the PS94 cruise, a six-component model (C2) was optimized based on spectral loadings, residual examination, and split-half validation using a convergence criterion of $1e^{-8}$ (Figure S2b in Supporting Information S1). The components were labeled based on their emission maxima: $C2_{411}$, $C2_{456}$, $C2_{404}$, $C2_{492}$, $C2_{338}$, and $C2_{302}$.

The spectral characteristics of each component were compared to those from several previous studies using the OpenFluor database (Murphy et al., 2014; Table S1, S2 in Supporting Information S1).

2.3. Lignin Phenols Analysis

The sum of concentrations of nine lignin phenols (TDLP9) is reported in this study, including p-hydroxyls (p-hydroxybenzaldehyde, p-hydroxy acetophenone, p-hydroxybenzoic acid), vanillyls (vanillin, acetovanillone, vanillic acid), and syringyls (syringaldehyde, acetosyringone, syringic acid). To measure the lignin phenols, unfiltered seawater samples containing 30 µg of DOC were acidified to pH 2.5 using concentrated HCl (reagent grade) and extracted onto 1 g reversed-phase (C18) sorbent cartridges using a Dionex Autotrace 280 Solid-Phase Extraction instrument. Lignin phenol analysis was performed following the method of Yan and Kaiser (2018a, 2018b). It allows the quantification of dissolved lignin phenols in small volumes of seawater (<200 mL) using alkaline $CuSO_4$ at 150°C. Ultra-high performance liquid chromatography with mass spectrometry detection in dynamic Multiple Reaction Monitoring mode and isotopically labeled surrogate standards were used for the detection and quantification of monomeric lignin phenols.

2.4. Dissolved Organic and Inorganic Carbon

DOC concentrations were determined using a Shimadzu TOC-L, according to Halewood et al. (2010); all samples were filtered at the time of collection using 0.2 µm pore size. The data are available online (Hansell, 2017, 2021). The accuracy was confirmed by measuring deep-water standards from the Consensus Reference Waters (Hansell, 2005). DOC measurements from both cruises (GN01 and PS94) were done at the Rosenstiel School of Marine and Atmospheric Sciences, University of Miami; they were consistent at the crossover stations.

Dissolved inorganic carbon (DIC) concentrations were measured using the methods of Woosley et al. (2017) and Ulfsbo et al. (2018). A description of the two cruises and the uncertainty analyses were discussed in Charette et al. (2020).

2.5. Trace Metal Data

Dissolved Fe and other TE data were obtained from Jensen et al. (2019) for GN01 Zn, Zhang et al. (2020) for GN01 Cd, Jensen, et al. (2019, 2020, 2022) for GN01 Fe and Mn, Gerringa et al. (2021) for GN04 trace metals, and Jensen et al. (2022) for GN01 Cu and Ni. Sample collection and analyses followed GEOTRACES protocols (Cutter et al., 2010, 2014; Rijkenberg et al., 2018).

Table 1

End-Member Values Used in Mass Balance Calculations (From Newton et al., 2013)

Water mass	Salinity	$\delta^{18}O$ [‰]	Arctic N:P (ANP)
Atlantic (Atl)	34.92	0.3	0
Pacific (Pac)	32.5	−1.1	1
Meteoric (Met)	0	−19	0
Sea-ice melt (SIM)	4	Surface +2.6	Surface

2.6. Linear Mixing Model

To study the pathways of DOM and TEs in the Arctic Ocean, the fractions of seawater with Pacific (f_{Pac}) and Atlantic (f_{Atl}) origin, sea ice melt (f_{SIM}), and meteoric water (f_{Met}) were determined based on the salinity (S), $\delta^{18}O$-H_2O (stable oxygen isotope ratio in water), and the Arctic N-P tracer (ANP, Newton et al., 2013). Mass balance for total mass and these four tracers are combined into the following system of linear equations, which is solved for each sample:

$$f_{Pac} + f_{Atl} + f_{SIM} + f_{Met} = 1 \tag{1}$$

$$f_{Pac}[S_{Pac}] + f_{Atl}[S_{Atl}] + f_{SIM}[S_{SIM}] + f_{Met}[S_{Met}] = [S]_{measured} \tag{2}$$

$$f_{Pac}\left[\delta^{18}O_{Pac}\right] + f_{Atl}\left[\delta^{18}O_{Atl}\right] + f_{SIM}\left[\delta^{18}O_{SIM}\right] + f_{Met}\left[\delta^{18}O_{Met}\right] = \left[\delta^{18}O\right]_{measured} \tag{3}$$

$$f_{Pac}[ANP_{Pac}] + f_{Atl}[ANP_{Atl}] + f_{SIM}[ANP_{SIM}] + f_{Met}[ANP_{Met}] = [ANP]_{measured} \tag{4}$$

"Meteoric" water is a combination of runoff and in situ precipitation. "Sea ice melt" is the net meltwater fraction, and does not distinguish between sequential passage into and out of the solid phase. Negative SIM is associated with net sea ice formation (i.e., the fraction of freshwater extracted from a seawater parcel into the solid phase). The end-member (water sources) values used in the calculations are presented in Table 1. The isotope data were from Pasqualini et al. (2017) and Paffrath et al. (2021). The limitations of the method and choices of end-members are discussed in detail in Newton et al. (2013) and Charette et al. (2020). We note here that the most significant errors in the method are known to be in the separation of Atlantic and Pacific water masses, which rely on nutrient combinations that are only quasi-conserved in the near-surface ocean. Current discussions of these issues, and novel suggestions for improvement, can be found in Alkire et al. (2019), Paffrath, et al. (2021), and Whitmore et al. (2020). High fractions of Pacific water in the TPD may actually originate from within the Chukchi and Siberian shelves instead (Bauch et al., 2011). Novel results based on rare earth elements concentrations and Nd isotopes confirm this assumption (Paffrath et al., 2021) and show that high Pacific water fractions in the TPD (Figure 2) can be an error of the method.

3. Results

3.1. Water Fractions

The four basic water fractions identified for the Arctic Ocean (Atlantic water, Pacific water, meteoric water, and sea-ice melt water), based on salinity, $\delta^{18}O$, and the ANP (Newton et al., 2013), indicated that up to 95% of the water in the central Nansen Basin originated from the Atlantic Ocean (Figure 2). In the Canada, Makarov and Amundsen Basins, AW occupied depths underneath the Pacific Water (PW) layer, while PW dominated the top 100–250 m (Figure 2). The distribution of AW and PW in the TPD was not correctly reflected by the ANP method alone and erroneously overrepresented the Pacific component (Paffrath et al., 2021). The Beaufort Gyre convergence results in a deepening of the upper boundary of the AW in the Canada Basin and its shoaling in the Makarov Basin (Zhong & Zhao, 2014). The border between the UHC and LHC roughly corresponded to the isopycnal of 27 kg/m³ (where f_{Pac} and f_{Atl} each account for ~50% of water), which was also the density surface of the in situ CDOM fluorescence maximum (Figure 3, Figure S3 in Supporting Information S1).

Sea-ice melt water (f_{SIM}) constituted 5% of the PML in the Canada and Nansen Basins. A brine signal (negative f_{SIM}) was detected within the TPD system and the upper 100 m of the Makarov and Amundsen Basins. According to the computed fractions, the halocline layers were also affected by brine formation. The PML shows great variation in the sea-ice meltwater fraction (f_{SIM}), along sections A and B, and between the two, with f_{SIM} ranging from −8% to +7%. In both the UHC and LHC waters sea-ice formation (brine enrichment, negative f_{SIM}) dominated, with f_{SIM} being more negative in the upper than lower layer (Figure 2). The PML in the Canada, Makarov, and Amundsen Basins exhibited a significant (up to ~22%) contribution of meteoric water (f_{Met}). The surface waters of these basins are strongly influenced by the TPD, which carries freshwater from the Siberian shelves. In addition to river discharge, the water mass calculations indicated that these waters had experienced ice melt, ice formation, and brine rejection.
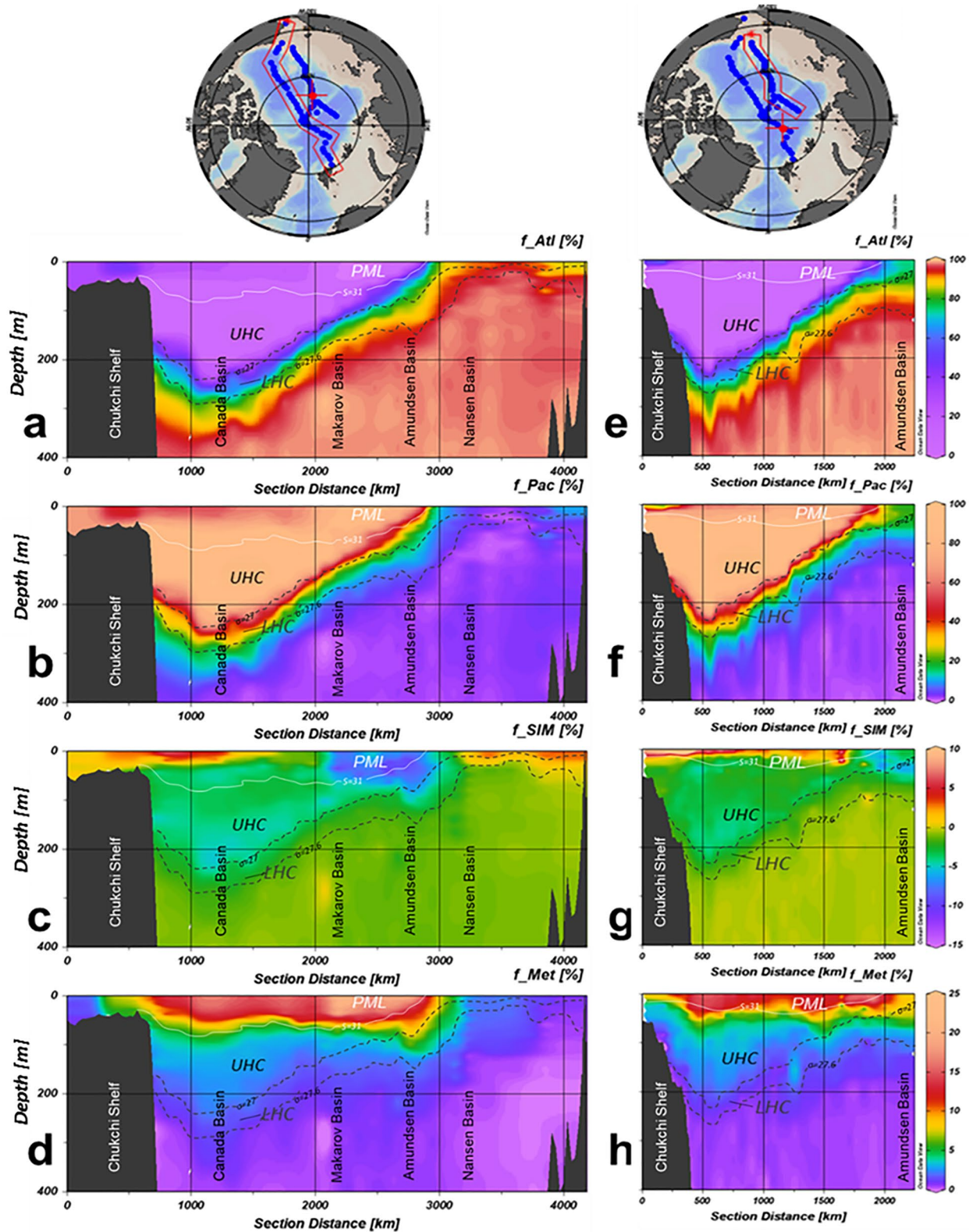
Figure 2. Calculated fractions of f_{Atl} (a, e), f_{Pac} (b, f), f_{SIM} (c, g) and f_{Met} (d, h) for Sections A and B, respectively. The white line represents the isohaline of $S = 31$, which is the border of the polar mixed layer (PML) in the Canada Basin. Black dashed isopycnal of $\sigma = 27$ kg/m^3 represents the lower/upper halocline (LHC/UHC) border. The LHC is bordered at the bottom by the isopycnal of $\sigma = 27.6$ kg/m^3. The color bar scales are different in each Panel.
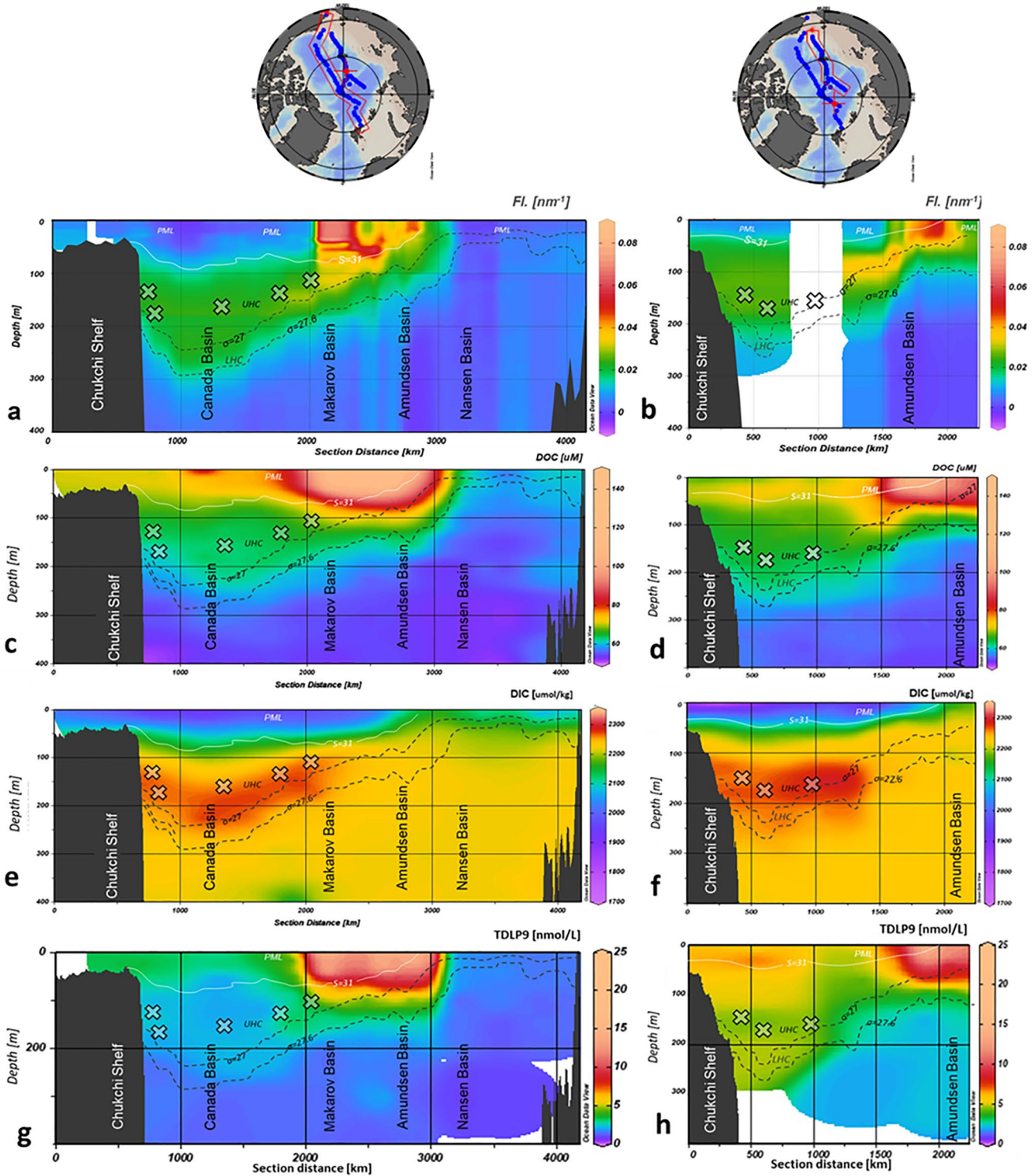
Figure 3. In situ chromophoric DOM (CDOM) fluorescence (Fl.; (a, b), dissolved organic carbon (DOC; (c, d), dissolved inorganic carbon (DIC, (e, f) and lignin phenols (TDLP9; (g, h) concentrations for sections A (a, c, e, g) and B (b, d, f, h) in the upper 400 m. The white line represents the isohaline of $S = 31$, which is the border of the polar mixed layer (PML) in the Canada Basin. Black dashed isopycnal of $\sigma = 27$ kg/m^3 represents the upper/lower halocline (LHC/UHC) border in the Canada Basin. The LHC is bordered at the bottom by the isopycnal of $\sigma = 27.6$ kg/m^3 in the Canada Basin. The silicate maximum (X) marks the core of the UHC according to Anderson et al. (2013). The color bar scales are different in each panel.

3.2. CDOM Fluorescence

In situ CDOM fluorescence was highly variable in the different Arctic Ocean basins (Figure 3), especially within the upper 400 m of the water column, but showed a very distinct pattern. Starting from the east, CDOM was consistently low throughout the water column of the Nansen Basin (<0.01 nm^{-1}; Figure 3). In the Central Arctic, the hydrography of the surface waters are governed by the TPD circulation, and the upper 70 m are characterized by very high in situ CDOM fluorescence (~0.08 nm^{-1}; Charette et al., 2020). The elevated fluorescence signal can be traced to a depth of 210 m in the Makarov and Amundsen Basin and to about 180 m above the Lomonosov ridge (Figure 3).

In contrast, in the Western Arctic, the in situ CDOM fluorescence was very low in surface waters of the Canada Basin (<0.01 nm^{-1}), but elevated deeper in the UHC and LHC, consistent with previous studies (e.g., Gao & Guéguen, 2018; Shen et al., 2016). A maximum in in situ CDOM fluorescence was detected at the UHC/LHC interface (roughly corresponding to the isopycnal $\sigma = 27$ kg/m^3, Figure 3), about 50 m below the UHC core as defined by the depth of the nutrient maximum (Figure 3, Figure S3e in Supporting Information S1). The LHC was also characterized by elevated in situ CDOM fluorescence compared to the underlying AW (Figures 3a and 3b). The in situ CDOM fluorescence signal closely follows the density structure in the water column, e.g., isopycnal of $\sigma \sim 27.6$ kg/m^3 coincided with the lower border of the CDOM trace (Figure 3).

3.3. Dissolved Organic Carbon

Similar to in situ CDOM fluorescence, total DOC concentrations were low throughout the water column (48–63 µmol/L) in the Nansen Basin (Figure 3). Within the TPD region, DOC concentrations were higher (up to 138 µmol/L) but limited to <170 m in the Amundsen Basin. In the Canada Basin, the distribution of DOC concentrations was different from CDOM. The former was enriched in the surface of the central Canada Basin (42–73 µmol/L) and decreased with depth. In contrast to CDOM, the DOC concentration was not elevated within the halocline. Below the halocline, AW had low CDOM and low DOC. Surface waters of the Canada Basin in Section B (which is closer to the Eurasian shelves) had more DOC than Section A by ~7 SµM.

3.4. Dissolved Inorganic Carbon

DIC concentrations were very low at the surface (<1950 µM; Figure 3), similar to in situ CDOM fluorescence (except without the TPD maximum), and enriched in the UHC (up to ~2300 µM). The maximum concentrations of DIC generally coincided with the nutrient maximum marking the core of the UHC (Figure 3). Within the TPD, the trend was the opposite to in situ CDOM fluorescence, as the surface of the Makarov and Amundsen Basins was depleted in DIC (~1960 µM). The Atlantic inflow in the eastern Arctic had higher DIC than the Pacific inflow at the Chukchi shelf (Figure 3).

3.5. Lignin Phenols

The high salinity (>34.7) waters of Atlantic origin dominating the eastern Arctic's Nansen Basin were characterized by low concentrations of lignin phenols (<3 nmol/L; Figure 3). In the Central Arctic, the importance of tDOM within the TPD was confirmed by the high lignin phenol concentrations (up to 21 nmol/L). In the Canada Basin, the vertical gradient was different for the distributions of DOM fluorescence and total DOC concentrations. Lignin phenol concentrations reached 5 nmol/L at the surface of the Canada Basin, decreased within the UHC, and were slightly enriched at the UHC/LHC interface. In general, Section B was characterized by higher lignin concentrations than Section A (Figure 3); overall, lignin phenol concentrations were ~5 nmol/L higher in Section B, closer to the Eurasian shelves.

3.6. Fluorescent Components of DOM

Based on the laboratory spectrofluorometric measurements, two PARAFAC models were developed: a four-component model for the GN01 data set (Canada Basin, C1) and a six-component model for the PS94 data set (Amundsen, Makarov and Nansen Basins, C2). Of all the fluorophores observed in the Canada Basin in this study, component $C1_{482}$ was earlier described as an ideal terrigenous tracer, for example, in Arctic boreal lakes

(Kothawala et al., 2014) and the Arctic Ocean (Walker et al., 2009; Williford et al., 2021). In the Canada Basin, $C1_{482}$ had the strongest correlation with lignin phenol concentrations, confirming its terrigenous origin. The maximum $C1_{482}$ fluorescence was observed at the very surface of the Canada Basin and in the UHC. Component $C1_{434}$ previously identified as marine humic (Kothawala et al., 2014), was highly correlated with DOC and lignin phenol concentrations (Figure 4).

$C1_{402}$, another humic-like component, has been observed spreading from the Chukchi Sea shelf to the core of the UHC in the Canada Basin and likely originates from marine organic matter decomposition in surface sediments on the shelf (Chen et al., 2018). The distribution of the only protein-like component $C1_{348}$ in the Canada Basin was like that of $C1_{402}$, but with a more pronounced fluorescence signal closer to the Chukchi Sea shelf.

Among all the fluorophores identified in the Nansen, Amundsen, and Makarov Basins, components $C2_{411}$, $C2_{456}$, $C2_{404}$, and $C2_{492}$ were humic-like, while $C2_{338}$ and $C2_{302}$ had a protein-like signature. $C2_{411}$ had the highest fluorescence intensity and is usually suggested to be produced in the water column (Yamashita et al., 2013). The two fluorescent components, $C2_{456}$ and $C2_{492}$, are usually described to be of terrigenous origin (Kothawala et al., 2014; Williford et al., 2021; Yamashita et al., 2013). These components had the strongest correlations with lignin phenol concentrations (Figure 4). $C2_{456}$ is commonly found in the Arctic Ocean and was reported in surface waters of the central Arctic, close to the Mackenzie River mouth and the Amundsen Gulf (Guéguen et al., 2015), and in the Lena River (Gonçalves-Araujo et al., 2015). $C2_{492}$ has a longer emission wavelength than $C2_{456}$, indicating molecules with higher molecular weight and higher hydrophobicity (Helms et al., 2008). Relative to $C2_{456}$, $C2_{492}$ has a higher molecular weight and therefore is more prone to flocculation, and its fluorescence intensity in the TPD region and the LHC was lower but relatively higher on the shelf. $C2_{492}$ fluorescence co-varied with dFe in boreal lakes (Kothawala et al., 2014). Similar to $C1_{402}$, the fourth humic component (third by intensity), $C2_{404}$, resembled a fluorescence signal that had been observed near the Chukchi Sea shelf and in the core of the UHC in the Canada Basin (Chen et al., 2018; Williford et al., 2021). The tryptophan-like $C2_{338}$ and the tyrosine-like $C2_{302}$ components have been reported in Arctic surface waters (Chen et al., 2018; Stedmon, Thomas, et al., 2011; Williford et al., 2021). Previously, $C2_{338}$ was reported as related to sea-ice CDOM and brine concentration (Stedmon, Thomas, et al., 2011). The tyrosine-like $C2_{302}$ was reported to be derived partly from the shelf and slope sediments (Chen et al., 2018).

In the Amundsen and Makarov basins, PARAFAC components $C2_{411}$ and $C2_{456}$ dominated the fluorescence signal in the PML and the UHC, LHC of the Makarov basin. $C2_{338}$ and $C2_{492}$ were slightly elevated in the PML and the halocline. $C2_{411}$ and $C2_{338}$ had the highest fluorescence intensity in the PML, while terrigenous $C2_{456}$ and $C2_{492}$ were most elevated at about 20 m depth at the upper boundary of the UHC.

The fluorescence intensity of all PARAFAC components was low in the Nansen Basin. The protein-like components were slightly elevated at the surface of the northern Nansen Basin (Amundsen Basin side). The Svalbard slope was also characterized by a slight increase in the fluorescence intensity of all the components.

3.7. Trace Metals

The TE distributions in the GN01 and GN04 Arctic GEOTRACES sections have been presented previously (Gerringa et al., 2021; Jensen et al., 2019, 2020; Zhang et al., 2019)). In this manuscript, we focus on potential relationships between the TEs and the various types of DOM indicators. The dFe, dNi, and dCu, concentrations in the surface waters of the TPD region were high compared to those in the Canada BasinsBasin (Figure 5)), and they showed strong to moderate correlations with lignin phenol concentrations, as well as optical indicators of tDOM ($C1_{482}$, $C2_{492}$; Figure 4, Figure S7 in Supporting Information S1). Other trace metals (dZn, dMn, dCd) did not exhibit correlations with the tDOM indicators.

In the Canada Basin, the PML was enriched in dNi, dCu, dCd, and dMn (Figure S7 in Supporting Information S1). Dissolved Cu was the only trace metal to show a significant correlation with DOC concentrations and protein-like fluorescence in the topupper 300 m of the Canada Basin (Figure S7 in Supporting Information S1). Interestingly, the correlation between f_{Met} and dCu was strong, but there was no significant correlation between dCu and CDOM.

The UHC waters were enriched in the dZn, dNi, dCu and dCd. These metals showed moderate correlations with optical sediment signal. The scavenging-prone dFe and dMn are rapidly lost, moving away from the continental
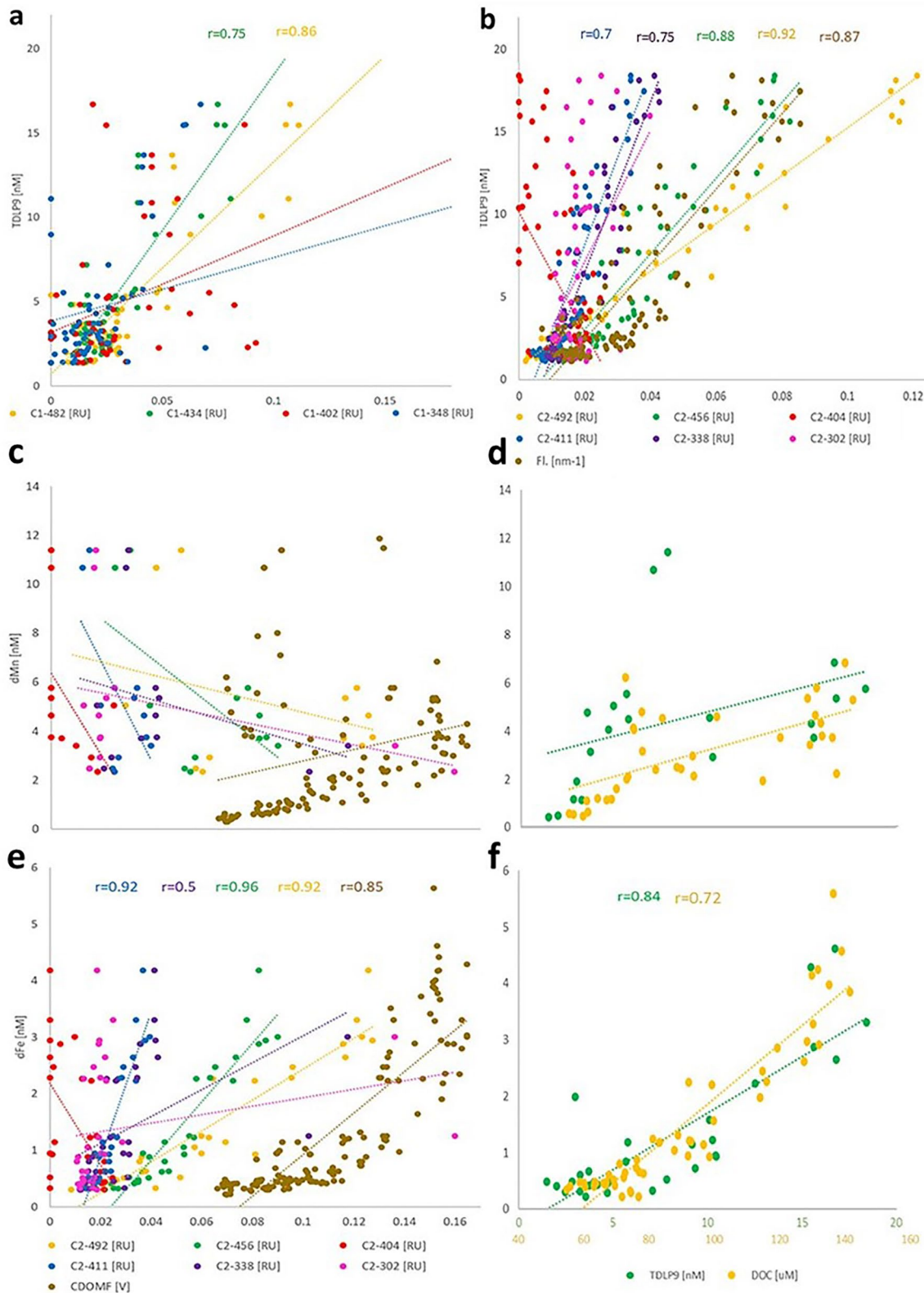
Figure 4. Correlation plots between the lignin phenol concentrations and C1 Parallel Factor Analysis (PARAFAC) components (a), C2 PARAFAC components, and in situ chromophoric DOM (CDOM) fluorescence (Fl.) (b), in the top 300 m of the Arctic Ocean. Scatterplots between the dMn (c, d), dFe (e, f), and C2 PARAFAC components and in situ CDOM fluorescence (CDOMF; c, e), lignin phenols (TDLP9) and dissolved organic carbon (DOC; d, f), in the top 300 m of the Arctic Ocean. Only significant correlations ($p < 0.001$ are shown).
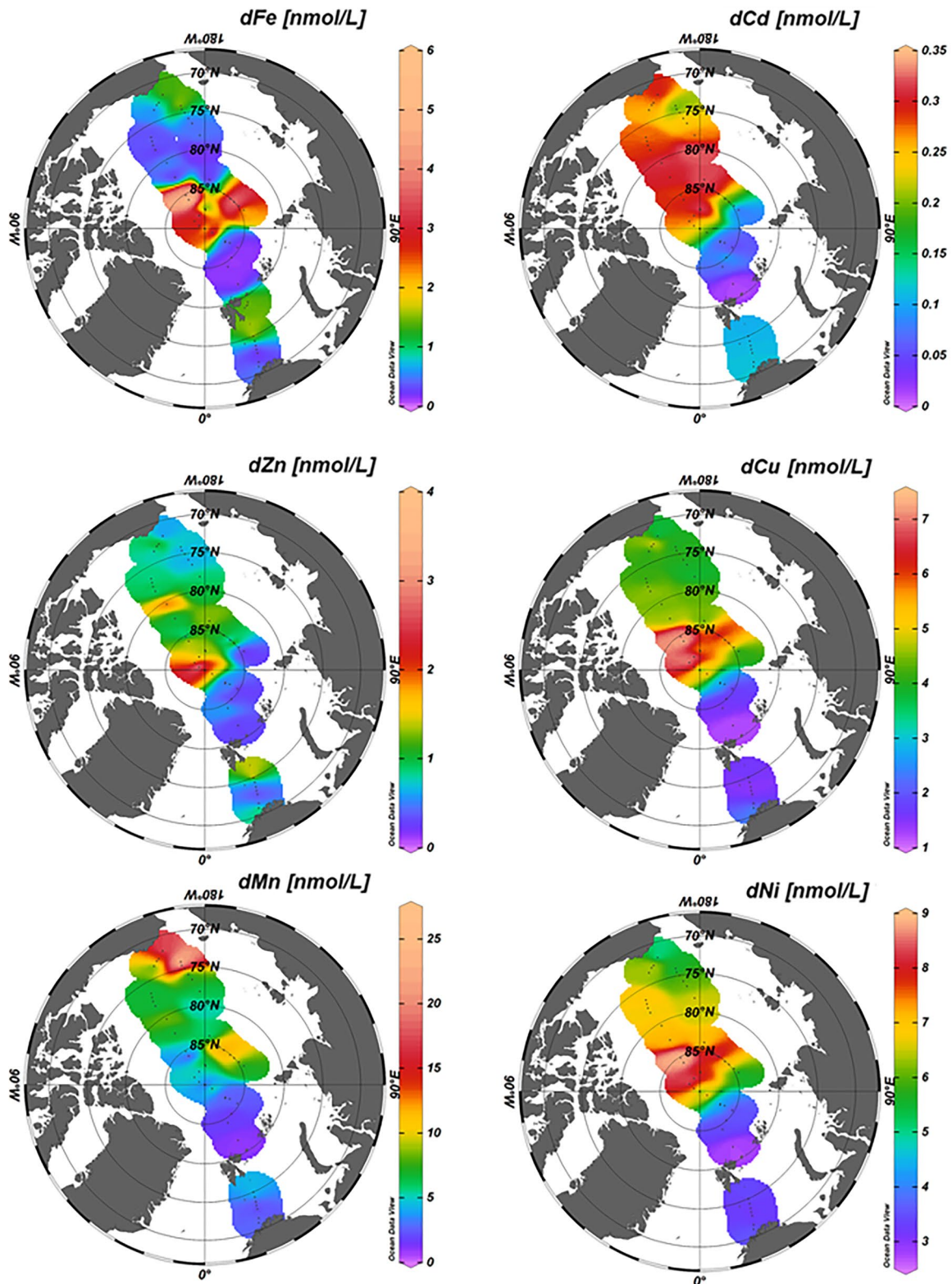
Figure 5. Concentrations of dFe, dMn, dNi, dCu, dZn, dCd in surface sample. The trace element (TE) distributions data for the GN01 and GN04 Arctic GEOTRACES sections have been published previously (Gerringa Loes et al., 2018, Gerringa et al., 2021; Jensen et al., 2019, 2020; Zhang et al., 2019).

slope (Figures S5 and S6 in Supporting Information S1, Jensen et al., 2020). Dissolved Fe exhibited weak to absent complexation to degraded UHC marine DOM in the UHC.

4. Discussion

We characterize the surface Arctic Ocean into three geographic regions based on the distribution of DOC, lignin, and optical properties. These three regions are physically separated by circulation and experience different sources of organic matter. The Eastern Arctic's Nansen Basin/Atlantic Eurasian shelf region is strongly influenced by AW and north-flowing Eurasian shelf waters carrying significant quantities of freshwater, nutrients, DOM, and sediments into the Arctic Ocean (Holmes et al., 2019; Rudels, 2015; Sholkovitz & Copland, 1981; Walker et al., 2013). The buoyant, low-salinity fluvial discharge mixed with the Atlantic water creates an upper ocean flow from the shelves to the central Arctic Ocean (Rennermalm et al., 2006). Arctic shelf waters are diverted by the Coriolis force to form a circumpolar anti-clockwise current shaped by coastal geometry resulting in multiple branches (Carmack et al., 2016; Horner-Devine et al., 2015). Below these upper waters is the LHC, which is believed to be formed via two mechanisms: a convective formation implying salinification of cold and fresh surface water and melting of sea ice as Atlantic water enters the ice-covered Arctic shelves, and an advective formation involving the cold and saline shelf water spreading into the deep Arctic basins (Kikuchi et al., 2004; Metzner et al., 2020).

The second region is the central Arctic that consists of the Amundsen and Makarov basins. In these basins, DOM distributions are influenced by the TPD, which connects the Eurasian shelves to the Fram Strait through surface advection (Charette et al., 2020). A clear tDOM signature is known to characterize the TPD region (Amon, 2004; Opsahl et al., 1999; Paffrath et al., 2021; Slagter et al., 2019; Williford et al., 2021).

On the Western Arctic's side of the TPD, the Chukchi shelf and Canada Basin are influenced by the advection of the relatively fresh ($S < 33$) nutrient-rich waters from the Pacific (Woodgate et al., 2012), which are modified on the shallow Chukchi shelf by the exchange with sediments (Kondo et al., 2016; Nakayama et al., 2011; Nishimura et al., 2012). Concentrations of tDOM and CDOM are much lower compared to the Eurasian Arctic and the TPD (Figure 3). The UHC is derived from PW inflow, and it lies on top of the LHC, with its core identified by high silicate concentration (Jones & Anderson, 1986; Figure S3 in Supporting Information S1). Atmospheric forcing creates the anticyclonic (i.e., convergent) Beaufort Gyre in the Canada Basin (Figure 1; Morison et al., 2021), deepening the nutricline and chlorophyll maximum in the Canada Basin interior (McLaughlin & Carmack, 2010). This anticyclonic circulation of surface waters is also found in the UHC of the Canada Basin, while the LHC seems to share a cyclonic circulation pattern with the Atlantic layer (Paqualini, 2021).

4.1. Distribution of Terrigenous DOM (tDOM)

Fluvial discharge is an important source of DOM to the Arctic Ocean (Amon, 2004; Anderson & Amon, 2015; Holmes et al., 2019; Opsahl et al., 1999; Walker et al., 2013). In the Amundsen and Makarov Basins, the concentrations of tDOM indicators were elevated in the upper 70 m, the waters most heavily influenced by the TPD (Figure 3). Besides the humic-like components of terrigenous and marine origin, the protein-like fluorescence exhibited a high correlation with the lignin concentration (Figure 4). This is explained by the fact that tannins and lignins, known for their protein-binding capability, can contribute to the protein-like fluorescence signature (Maie et al., 2008).

The terrigenous contribution to DOM distinguishes the Arctic Ocean from other oceans (Anderson & Amon, 2015), as reflected in the strong correlation between DOC and lignin phenols (rr = 0.91, $p < 0.001$). In situ CDOM fluorescence had a similar correlation with lignin phenol concentrations as with DOC (Figure 4b). The correlation between lignin phenols and f_{Met} was weaker in the Canada Basin than in the Amundsen, Makarov and Nansen Basins (Figures 4a and 4b), indicating that fluvial discharge plays a more prominent role in the DOM pool within the TPD and on the Eurasian side of the TPD. In situ CDOM fluorescence is a powerful, high vertical resolution and real-time indicator of the TPD location. The broad distribution of this current feature between the Lomonosov and Alpha Ridges shown here was also observed in 1998, 2005 (unpublished data), and 2007 (Williford et al., 2021).

The Arctic shelves, particularly the Chukchi shelf, are characterized by elevated seasonal primary productivity where sediments can serve as a source of diagenetically altered DOM (Cooper et al., 2005). The water fractions combined with the fluorescent components of DOM indicate to lateral shelf—basin transport. The UHC contains up to 100% of f_{Pac}, and the LHC contains up to 85% of f_{Atl} (Figure 2). The UHC exhibits a higher brine content (up to 5% negative SIM, indicative of excess brine) than the LHC, but both have a more negative f_{SIM} compared to the PML and the AW. Elevated concentrations of the sediment-derived fluorophores $C1_{402}$ and $C2_{404}$ (Chen et al., 2018; Williford et al., 2021) were observed in the UHC. This signal likely originates from marine organic matter decomposition in surface sediments on the shelf, consistent with a significant correlation between $C1_{402}$ fluorescence intensity and DIC concentration in the Canada Basin ($r = 0.7$, $p < 0.001$). The UHC showed a pronounced CDOM signature but low lignin and other tDOM proxy concentrations and high nutrient and DIC concentrations (Figure 3), the latter two indicating organic matter degradation in source waters. The depth-integrated levels of in situ CDOM fluorescence and DOC concentration are lower in the LHC than in the UHC, but they are high compared to AW. The concentration of marine component $C2_{411}$ was higher in the UHC compared to the LHC, but the concentration of the terrigenous component $C2_{456}$ was higher in the LHC relative to the UHC.

The terrigenous signal in the LHC and the LHC/UHC interface suggests lateral transport of organic matter from the Eurasian shelves into the interior Arctic via the LHC formation process. Lignin phenol concentrations and in situ CDOM fluorescence peaked at the UHC/LHC interface ($\sigma = 27.6$ kg/m^3). The in situ CDOM fluorescence signal closely follows the density structure in the water column (Figure 3), indicating that physical processes (e.g., sea ice formation/melt processes) have a major effect on the DOM distribution in the Arctic Ocean.

In the Western Arctic, the PML of the Canada Basin was depleted in tDOM indicators. The Beaufort Gyre alters the biogeochemical conditions of the PML layer in the Canada Basin. The layer contains up to 5% of ice melt but is dominated by the f_{Pac} (McLaughlin et al., 2004). According to the oxygen isotope and salinity calculations, the Canada Basin PML also contained up to ∼16% of meteoric water, often explained by river discharge (Jensen et al., 2019; Jones et al., 2008; Proshutinsky et al., 2019; Yamamoto-Kawai et al., 2008, 2009). However, a direct riverine source is not supported, given the low concentrations of lignin phenols and fluorescent terrigenous proxies. The river water must have undergone at least one sea-ice formation/melting cycle that diminished the tDOM signal. The Mackenzie River input is mostly exported to the Archipelago, only entering the central Arctic occasionally (approximately once every 4 years; Fichot et al., 2013). The DOC concentrations were relatively high in the PML compared to halocline waters, but in situ CDOM fluorescence was very low (Figure 3), indicating the presence of non-fluorescent substances in surface waters of the Canada Basin, which are mostly of marine origin (Shen et al., 2016; Wang et al., 2006).

4.2. Processes Affecting the Distribution of DOM in the Arctic Ocean

We consolidated data from all water masses, and the in situ CDOM fluorescence correlates better with f_{SIM} than with f_{Met} ($r = -0.6$, $r = 0.5$, respectively, $p < 0.001$, Figure 5), despite the fact that fluvial discharge is the largest source of CDOM to the Arctic Ocean (Amon, 2004; Anderson & Amon, 2015; Stedmon, Amon, et al., 2011, 2011b; Walker et al., 2009; Williford et al., 2021). The correlation between f_{SIM} and in situ CDOM shows that sea ice formation/melt processes largely control the distribution of DOM in the Arctic Ocean, consistent with a recent study by Hölemann et al. (2021) who demonstrate that fluvial discharge is rapidly diluted by the melting of land fast ice during the spring freshet. In addition, river water undergoes at least one freeze-melt cycle on the Arctic shelf seas before entering the TPD. The mean residence time of river-runoff on the Siberian shelves is about 5 ± 2 years (Schlosser et al., 1994). During the shelf transition, the water is imprinted with a specific oxygen isotope and salinity signature that is later carried into the central basins of the Arctic Ocean, mostly in the TPD region. The difference in negative f_{SIM} between section A, crossing the Arctic Ocean at the North Pole, and section B, situated closer to the Eurasian shelves, is likely due to the pulsed release of shelf water within the TPD system (Bauch et al., 2011; Kaiser et al., 2017; Karcher et al., 2012; Thibodeau & Bauch, 2015; Thibodeau et al., 2014).

The strongest correlation between f_{Met} and lignin phenol concentrations was observed in the TPD region of the Amundsen and Makarov Basins ($r = 0.96$, $r = 0.92$, respectively; $p < 0.001$; Figure 6). A weaker correlation was found between lignin phenols and f_{Met} in the Nansen Basin (Figure S4 in Supporting Information S1). No correlations between these parameters were observed in the Chukchi Sea and the Canada Basin. The strong negative

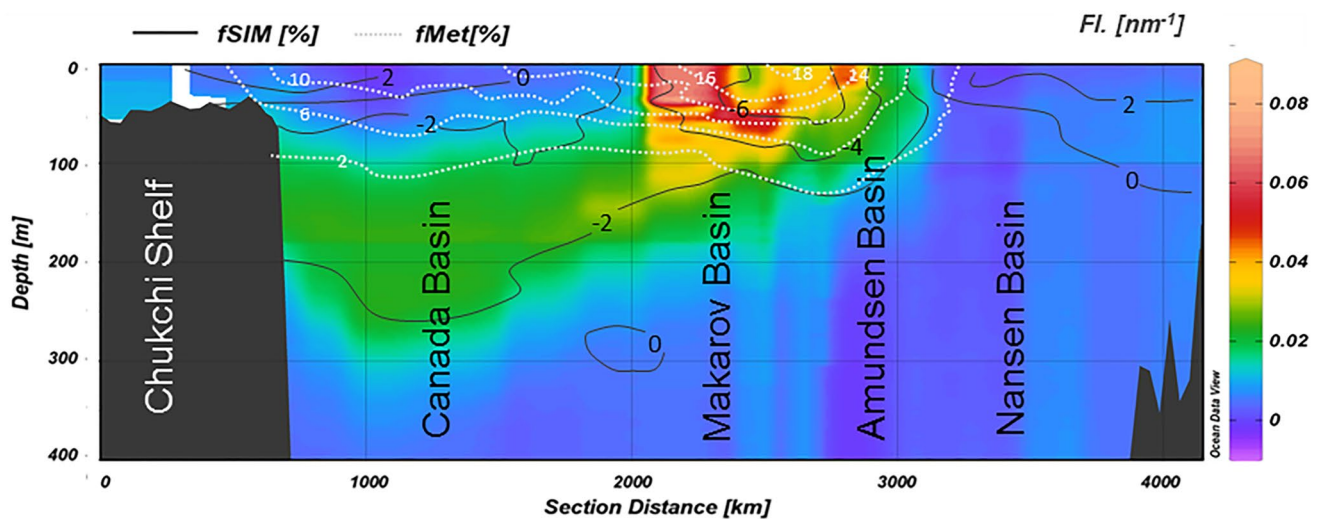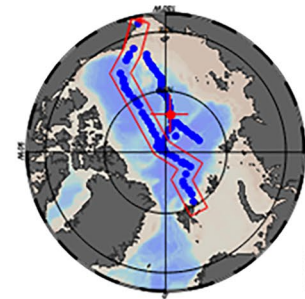| Basin	Pearson's correlation with fSIM	Pearson's correlation with fMet
Chukchi Shelf	-0.56	non-significant
Canada Basin	-0.59	non-significant
Makarov Basin	-0.78	0.76
Amundsen Basin	-0.79	0.85
Nansen Basin	-0.88	non-significant
All basins	-0.6	0.5

Figure 6. Top panel: relationship (Pearson correlation) of the in situ chromophoric DOM (CDOM) fluorescence (Fl.), with f_{SIM} and f_{Met} in the top 400 m of the Chukchi Sea, Canada, Makarov, Amundsen, and Nansen Basins. Only significant ($p < 0.001$) correlations are shown. Bottom panel: the in situ CDOM fluorescence for section A in the upper 400 m. The light gray dotted lines represent the f_{Met} isolines, and the solid black lines represent f_{SIM} isolines.

correlation between the f_{SIM} and lignin phenols in the central Arctic basins (Makarov and Amundsen) indicates substantial modification of river discharge on the Eurasian shelves during the freezing/melting/mixing processes before entering the open Arctic Ocean. This modification of Eurasian shelf water during sea-ice formation is reflected in elevated brine fractions (negative f_{SIM} values) along with high CDOM concentrations in the TPD (Figures 2, 3 and 5) and the halocline layers. Due to the very low salinity (high buoyancy) of the PML over the shelves, most of the tDOM-enriched brine is advected above the Atlantic layer. The general overlap of the in situ CDOM trace with the iso-contour lines of brine enrichment (fraction of sea ice) is a strong testament that the distribution of DOM, originating on the Arctic shelf seas, is at least partially controlled by sea ice formation and results in lateral advection of shelf DOM to the central Arctic Ocean. Such a mechanism has been suggested by Hölemann et al. (2021), who demonstrated that typical river signals on the Eurasian shelf are diluted and over-layered by freshwater from melting fast ice. All these processes on Arctic shelves also influence the distribution of trace metals that are complexed with dissolved organic ligands. As the Arctic warms, the sea-ice cycle over the shelves has already begun to change dramatically (Li et al., 2021). In the near term, the amplitude of the annual sea-ice freeze/melt cycle might increase along with brine formation. The impacts of these changes on Arctic productivity, carbon dioxide sequestration, and TE transport need to be monitored with repeat sampling campaigns.

4.3. Trace Metals in Relation to DOM and Hydrographic Features

The external sources controlling the TE distributions in the GN01 and GN04 Arctic GEOTRACES sections have been presented previously (Jensen et al., 2019, 2020; Zhang et al., 2019; Gerringa et al., 2021, Figure 5, Figures S5, S6 in Supporting Information S1). Nonetheless, one of the goals of this study was to compare the distributions of TEs with those of DOM components in order to understand how organics might control TE distributions

in the Arctic Ocean. Several factors are known to control the relationship between DOM and TE distributions. First, the long-distance transport of low-solubility trace metals, for example, Fe(III), heavily depends on complexation with organic ligands (Gledhill & Buck, 2012). In other cases, high correlation of the trace metal and DOM indicators can point to a common source and transportation mechanisms, for example, Mn(II) is present in free form in seawater (Byrne, 2002; Jensen et al., 2020), so it does not depend on binding to organic ligands to maintain solubility. Weak correlations between DOM and dissolved metals do not necessarily mean weak trace element-organic ligands associations, as, for example, the concentration of available ligands can greatly exceed the concentration of TEs. In addition, processes such as biological uptake and remineralization may affect the correlations between DOM and dissolved metals concentrations.

In the Central Arctic (TPD waters), lignin phenol concentrations, as well as optical indicators of tDOM (C1$_{482}$, C2$_{492}$), showed strong correlations with dFe and dCu (Figure 4, Figure S7 in Supporting Information S1) and a moderate correlation with dNi (Figure S7 in Supporting Information S1) due either to strong binding to terrigenous ligands within the DOM pool or a common point of origin and co-transport mechanisms.

The dFe correlation with DOC was lower than that with lignin (Figure 4), indicating preferential binding of dFe with tDOM. Previous studies have shown the association of dFe with humic-like terrigenous organic ligands, particularly in the TPD, and humic-like marine ligands (Laglera et al., 2019). Slagter et al. (2019) reported that humic substances are, in fact, the dominant type of Fe-binding organic ligand in the surface of the Arctic Ocean. While dFe and divalent dCu are known to be organically complexed in natural waters (Laglera et al., 2019; Semeniuk et al., 2015; Shank et al., 2004; Slagter et al., 2017, 2019; Williford et al., 2021), the organic chelation of dNi is less well understood (Vraspir & Butler, 2009). It appears that dNi can be partially complexed by strong organic ligands (logK = 17–19; Van den Berg & Nimmo, 1987; Morel & Price, 2003). Terrestrial humic substances have been suggested as the likely source of high-affinity, low abundance ligands for dCu (Muller & Batchelli, 2013). Another study reported that fluvial allochthonous organic matter dominated the strong complexation capacity of dCu in the Cape Fear River estuary (Shank et al., 2004). Indeed, compared to Fe and Ni, Cu likely prefers sulfur-containing ligands of lower molecular weight (Zhengbin & Liansheng, 1982). While we cannot know for sure that the correlations between the TEs and the organic compounds mean organic complexation, their strong correlations certainly warrant further investigation of the organic ligand binding of these riverine-derived metals as well as their behavior during sea ice formation. Other trace metals (dZn, dMn, dCd) did not appear to be transported across the TPD by tDOM binding.

The optical sediment signal (C1$_{402}$) showed moderate correlations with dFe, dNi, and dCu (Figure S8 in Supporting Information S1). The former, dFe, dissipated rapidly within the UHC moving offshore, while dNi, dCu, and C1$_{402}$ concentrations persisted in the central Canada Basin (Figures S5, S6 in Supporting Information S1). In the Chukchi Sea, brine rejection drives convection, creating dense, metal- and organic-rich bottom waters, which detrain from the shelf, feed the UHC, and spread along isopycnals across the Canada Basin (Mathis et al., 2007). The degraded shelf-derived DOM serves as a source of ligands to the UHC. The dZn (Jensen et al., 2019), dCd (Zhang et al., 2019), dCu, dNi (Jensen et al., 2022), and dMn (Jensen et al., 2020) have elevated concentrations throughout the UHC in the Canada Basin water column (Figures S5 and S6 in Supporting Information S1). The strong correlation of dCd, dZn, and dNi with C1$_{402}$ in the Canada Basin suggests the Chukchi shelf sediments are an important source of trace metals (Figure S8 in Supporting Information S1) as well as a source of strong organic ligands that bind to them and carry them offshore within the UHC. Indeed, in previous studies, dZn was shown to be strongly complexed (>95%) by organic ligands (Jakuba et al., 2012), especially sedimentary humic acids (Raspor et al., 1984; Sohn & Hughes, 1981) and low-molecular-weight thiols (Dupont & Ahner, 2005). Less is known about the potential organic ligands that bind to dCd, but prior studies have found that ~70% of the dCd in surface waters was strongly complexed (Bruland, 1992).

Dissolved Cu was the only trace metal to exhibit a significant correlation with DOC concentrations and protein-like fluorescence in the upper 300 m of the Canada Basin (Figure S7 in Supporting Information S1) and a negative correlation with DIC (Figure S8 in Supporting Information S1), suggesting dCu is likely complexed with marine DOM in the Canada Basin, consistent with previous findings that DOM derived from marine phytoplankton and cyanobacteria could be an important source of Cu ligands (Laglera & van den Berg, 2003; Nixon et al., 2019). Coccolithophorids release thiols in response to Cu addition (Croot et al., 2000), and thiol-like levels were associated with the chlorophyll-*a* maximum in the Canadian Archipelago and Canada Basin (Gao & Guéguen, 2018; Nixon et al., 2019). The high correlation between f_{Met} and dCu, but not between dCu and CDOM, is evidence

that the river water had been through at least one freezing cycle before reaching the Beaufort Gyre (there was no correlation between the lignin phenols concentrations and the f_{Met} in the Canada Basin). That is to say that the sea-ice formation/melting cycle in the Canada Basin strips out the tDOM signal, but the dCu content seems to be conserved due to the availability of algal-derived ligands, as indicated by the high correlation with DOC.

The scavenging-prone dFe and dMn are rapidly lost, moving away from the continental slope (Figures S5 and S6 in Supporting Information S1, Jensen et al., 2020). Dissolved Fe exhibits weak to absent complexation to degraded UHC marine DOM molecules, as opposed to a strong correlation to tDOM within the TPD current (Williford et al., 2021). Besides scavenging, dFe concentrations in the Canada Basin are moderated by light- and nitrate-limited biological uptake (Aguilar-Islas et al., 2013). Dissolved Mn shares common sources and sinks with dFe but has a different redox reactivity and speciation (Jensen et al., 2020; Middag et al., 2011). The correlations of dMn with in situ CDOM fluorescence, DOC, and lignin phenols were positive but statistically insignificant. As mentioned above, in contrast to dFe, whose solubility depends on organic complexation, most dMn in seawater is considered to exist in the free form (Byrne, 2002). In estuaries, dMn does not undergo significant salt-initiated coagulation or precipitation (Sholkovitz & Copland, 1981), but it is subject to bacterial precipitation (Sunda, 2012). Recent studies, however, show that humic ligands may play a greater role in dMn transport from coastal areas to the ocean than previously thought (Oldham et al., 2017, 2020).

The LHC exhibits relatively low concentrations of TEs (Figures S5 and S6 in Supporting Information S1; Gerringa et al., 2021) and similarly had low concentrations of DOM (Figure 2). The Eurasian shelves are generally deeper and less biologically productive than the Chukchi Sea shelf, reducing the amount of remineralized and diagenetically altered organic matter released from sediments (Jones & Anderson, 1986; Sakshaug, 2004). However, these shelves receive large amounts of tDOM, which might mask autochtonous DOM release from the sediments (Rijkenberg et al., 2018).

5. Conclusions

DOM is a valuable tracer of water masses and features of the Arctic Ocean. In the Amundsen and Makarov Basins, the concentration of tDOM was elevated in the upper 70 m of the water column due to the TPD. In contrast to the central Arctic basins, the PML of the Canada and Nansen Basins was depleted in tDOM. Underneath the PML, the UHC in the Canada Basin was marked by high DIC concentrations and a Chukchi-shelf-sediment-derived signature. The terrigenous signal found in the LHC and LHC/UHC interface demonstrates the lateral transport of organic matter from the Eurasian shelves into the Arctic interior via an advective LHC formation process. Sea-ice formation and melting processes shape the patterns of DOM distributions relative to hydrography and water mass tracers by separating DOM from river water. This has consequences for the interpretation of coupled physical/biogeochemical driving factors influencing source assignments for freshwater, DOM, carbon, as well as trace metal/DOM interactions.

The distributions and co-variation of TEs and DOM indicators in the Arctic Ocean provided novel insights about the complex interactions of marine biogeochemical cycles, potential metal-ligand interactions, and sea-ice formation and melting. Chukchi shelf sediments were the most important sources of dCd, dZn, and dNi, as well as sediment-derived organic ligands that bind and carry them offshore within the UHC in the Canada Basin. In contrast, dCu was associated with marine DOM in the PML and the UHC of the Canada Basin. Sediment-derived DOM did not appear to facilitate the long-range spreading of dFe into the UHC in the Canada Basin. On the other hand, tDOM molecules were found to be strong ligands for dFe, dNi, and dCu, facilitating their long-range transport from the Eurasian shelves to the central Arctic Ocean via the TPD system and eventually the East Greenland Current and the North Atlantic as suggested by the distribution of terrigenous CDOM in these waters (Amon et al., 2003) and a recent study in the Fram Strait (Krisch et al., 2022).

Qualitative DOM studies, for example, nuclear magnetic resonance, coupled with hydrography and trace metal distributions are necessary to further constrain biological utilization and growth as well as physical processes, such as freezing/thawing, advection, and particle scavenging. This study highlights the importance of understanding the biogeochemistry of DOM and its potential to provide insights about water mass transformations, freshwater sources, and the fate of TEs in the Arctic Ocean.

Data Availability Statement

The data collected during the U.S. Arctic GEOTRACES (GN01; Kadko & Landing, 2015) cruise are available in a consolidated form as part of the GEOTRACES Intermediate Data Product 2021, at https://www.geotraces. org/geotraces-intermediate-data-product-2021/. The data collected during the GEOTRACES TransARC II cruise (PS94; Rabe et al., 2016a, 2016b; Schauer, 2016) can be found at the PANGAEA data archive (https:// www.pangaea.de: https://doi.org/10.1594/PANGAEA.859558), the British Oceanographic Data Centre (http:// www.bodc.ac.uk/geotraces), and Biological and Chemical Oceanography Data Management Office (Landing et al., 2017, 2019). The dissolved organic carbon data are available online (Hansell, 2017, 2021). Dissolved Fe and other TE data were obtained from Jensen et al. (2019) for GN01 Zn, Zhang et al. (2020) for GN01 Cd, Jensen et al. (2019, 2020, 2022) for GN01 Fe and Mn, Gerringa et al., and Jensen et al. (2022) for GN01 Cu and Ni. The isotope data were from Pasqualini et al. (2017) and Paffrath et al. (2021).

References

Aguilar-Islas, A. M., Rember, R., Nishino, S., Kikuchi, T., & Itoh, M. (2013). Partitioning and lateral transport of iron to the Canada basin. *Polar Science*, *7*(2), 82–99. https://doi.org/10.1016/j.polar.2012.11.001

Ahmed, R., Prowse, T., Dibike, Y., Bonsal, B., & O'Neil, H. (2020). Recent trends in freshwater influx to the Arctic Ocean from four major Arctic-draining rivers. *Water*, *12*(4), 1189. https://doi.org/10.3390/w12041189

Alkire, M. B., Rember, R., & Polyakov, I. (2019). Discrepancy in the identification of the Atlantic/Pacific front in the central Arctic ocean: No versus nutrient relationships. *Geophysical Research Letters*, *46*(7), 3843–3852. https://doi.org/10.1029/2018GL081837

Amon, R. M. W. (2004). The role of dissolved organic matter for the Arctic Ocean carbon cycle. In "*The Arctic ocean organic carbon cycle: Present and past*". In R. Stein, & R. W. Macdonald (Eds.), (pp. 83–99). Springer.

Amon, R. M. W., Budeus, G., & Meon, B. (2003). Dissolved organic carbon (DOC) distribution and origin in the Nordic seas: Exchanges with the Arctic Ocean and the north Atlantic. *Journal of Geophysical Research*, *108*(C7), 3221. https://doi.org/10.1029/2002JC001594

Amon, R. M. W., Rinehart, A. J., Duan, S., Louchouarn, P., Prokushkin, A., Guggenberger, G., et al. (2012). Dissolved organic matter sources in large Arctic rivers. *Geochimica et Cosmochimica Acta*, *94*, 217–237. https://doi.org/10.1016/j.gca.2012.07.015

Anderson, L. G., & Amon, R. M. W. (2015). DOM in the Arctic Ocean. In *Biogeochemistry of marine dissolved organic matter* (pp. 609–663). Academic Press.

Anderson, L. G., Andersson, P. S., Björk, G., Peter Jones, E., Jutterström, S., & Wahlström, I. (2013). Source and formation of the upper halocline of the Arctic Ocean. *Journal of Geophysical Research: Oceans*, *118*(1), 410–421. https://doi.org/10.1029/2012jc008291

Bauch, D., van der Loeff, M. R., Andersen, N., Torres-Valdes, S., Bakker, K., & Abrahamsen, E. P. (2011). Origin of freshwater and polynya water in the Arctic Ocean halocline in summer 2007. *Progress in Oceanography*, *91*(4), 482–495. https://doi.org/10.1016/J.POCEAN.2011.07.017

Benner, R. (2011). Loose ligands and available iron in the ocean. *Proceedings of the National Academy of Sciences*, *108*(3), 893–894. https://doi.org/10.1073/pnas.1018163108

Benner, R., Louchouarn, P., & Amon, R. M. W. (2005). Terrigenous dissolved organic matter in the Arctic Ocean and its transport to surface and deep waters of the north Atlantic. *Global Biogeochemical Cycles*, *19*(2). https://doi.org/10.1029/2004gb002398

Berner, L. T., Massey, R., Jantz, P., Forbes, B. C., Macias-Fauria, M., Myers-Smith, I., et al. (2020). Summer warming explains widespread but not uniform greening in the Arctic tundra biome. *Nature Communications*, *11*(1), 1–12. https://doi.org/10.1038/s41467-020-18479-5

Bruhwiler, L., Parmentier, F. J. W., Crill, P., Leonard, M., & Palmer, P. I. (2021). The Arctic carbon cycle and its response to changing climate. *Current Climate Change Reports*, *7*(1), 14–34. https://doi.org/10.1007/s40641-020-00169-5

Bruland, K. W. (1992). Complexation of cadmium by natural organic ligands in the central north Pacific. *Limnology & Oceanography*, *37*(5), 1008–1017. https://doi.org/10.4319/lo.1992.37.5.1008

Butler, A., & Theisen, R. M. (2010). Iron (III)–siderophore coordination chemistry: Reactivity of marine siderophores. *Coordination Chemistry Reviews*, *254*(3–4), 288–296. https://doi.org/10.1016/j.ccr.2009.09.010

Byrne, R. H. (2002). Speciation in seawater. *Chemical speciation in the Environment*, 322–357. https://doi.org/10.1002/9780470988312.ch12

Carmack, E., McLaughlin, F., Yamamoto-Kawai, M., Itoh, M., Shimada, K., Krishfield, R., & Proshutinsky, A. (2008). Freshwater storage in the northern ocean and the special role of the Beaufort gyre. In *Arctic–subArctic ocean fluxes* (pp. 145–169). Springer.

Carmack, E. C., Yamamoto-Kawai, M., Haine, T. W., Bacon, S., Bluhm, B. A., Lique, C., et al. (2016). Freshwater and its role in the Arctic marine system: Sources, disposition, storage, export, and physical and biogeochemical consequences in the Arctic and global oceans. *Journal of Geophysical Research: Biogeosciences*, *121*(3), 675–717. https://doi.org/10.1002/2015jg003140

Charette, M. A., Kipp, L. E., Jensen, L. T., Dabrowski, J. S., Whitmore, L. M., Fitzsimmons, J. N., et al. (2020). The transpolar drift as a source of riverine and shelf-derived trace elements to the central Arctic Ocean. *Journal of Geophysical Research: Oceans*, *125*(5), e2019JC015920. https://doi.org/10.1029/2019JC015920

Chen, M., Jung, J., Lee, Y. K., & Hur, J. (2018). Surface accumulation of low molecular weight dissolved organic matter in surface waters and horizontal off-shelf spreading of nutrients and humic-like fluorescence in the Chukchi Sea of the Arctic Ocean. *Science of the Total Environment*, *639*, 624–632. https://doi.org/10.1016/j.scitotenv.2018.05.205

Cooper, L. W., Benner, R., McClelland, J. W., Peterson, B. J., Holmes, R. M., Raymond, P. A., et al. (2005). Linkages among Runoff, dissolved organic carbon, and the stable oxygen isotope composition of seawater and other water mass indicators in the Arctic Ocean. *Journal of Geophysical Research*, *110*(G2). https://doi.org/10.1029/2005jg000031

Cory, R. M., Miller, M. P., McKnight, D. M., Guerard, J. J., & Miller, P. L. (2010). Effect of instrument-specific response on the analysis of fulvic acid fluorescence spectra. *Limnology and Oceanography: Methods*, *8*(2), 67–78. https://doi.org/10.4319/lom.2010.8.67

Croot, P. L., Moffett, J. W., & Brand, L. E. (2000). Production of extracellular Cu complexing ligands by eucaryotic phytoplankton in response to Cu stress. *Limnology & Oceanography*, *45*(3), 619–627. https://doi.org/10.4319/lo.2000.45.3.0619

Cutter, G., Andersson, P., Codispoti, L., Croot, P., Francois, R., Lohan, M. C., & Rutgers vd Loeff, M. (2010). Sampling and sample-handling protocols for GEOTRACES cruises.

Cutter, G. A., Andersson, P. S., Codispoti, L., Croot, P. L., Francois, R., Lohan, M. C., et al. (2014). Sampling and sample-handing protocols for GEOTRACES cruises. Retrieved from http://www.geotraces.org/images/stories/documents/intercalibration/Cookbook_v2.pdf

Dupont, C. L., & Ahner, B. A. (2005). Effects of copper, cadmium, and zinc on the production and exudation of thiols by Emiliania Huxleyi. *Limnology & Oceanography*, *50*(2), 508–515. https://doi.org/10.4319/lo.2005.50.2.0508

Fichot, C. G., Kaiser, K., Hooker, S. B., Amon, R. M., Babin, M., Bélanger, S., et al. (2013). Pan-Arctic distributions of continental runoff in the Arctic Ocean. *Scientific Reports*, *3*(1), 1–6. https://doi.org/10.1038/srep01053

Fritz, M., Vonk, J. E., & Lantuit, H. (2017). Collapsing Arctic coastlines. *Nature Climate Change*, *7*(1), 6–7. https://doi.org/10.1038/nclimate3188

Gao, Z., & Guéguen, C. (2018). Distribution of thiol, humic substances and colored dissolved organic matter during the 2015 Canadian Arctic GEOTRACES cruises. *Marine Chemistry*, *203*, 1–9. https://doi.org/10.1016/j.marchem.2018.04.001

Gerringa, L. J. A., Rijkenberg, M. J. A., Slagter, H. A., Laan, P., Paffrath, R., Bauch, D., et al. (2021). Dissolved Cd, Co, Cu, Fe, Mn, Ni, and Zn in the Arctic Ocean. *Journal of Geophysical Research: Oceans*, *126*(9), e2021JC017323. https://doi.org/10.1029/2021jc017323

Gerringa Loes, J. A., Rijkenberg, M. J. A., & Slagter, H. A. (2018). Dissolved iron measured on board with Flow injection analysis and iron-binding dissolved organic ligands from Ultra Clean CTD collected depth profiles during GEOTRACES PS94 Arctic cruise on Polarstern. *PANGAEA*. https://doi.org/10.1594/PANGAEA.890975

Gledhill, M., & Buck, K. N. (2012). The organic complexation of iron in the marine environment: A review. *Frontiers in Microbiology*, *3*, 69. https://doi.org/10.3389/fmicb.2012.00069

Gonçalves-Araujo, R., Granskog, M. A., Bracher, A., Azetsu-Scott, K., Dodd, P. A., & Stedmon, C. A. (2016). Using fluorescent dissolved organic matter to trace and distinguish the origin of Arctic surface waters. *Scientific Reports*, *6*(1), 33978. https://doi.org/10.1038/srep33978

Gonçalves-Araujo, R., Stedmon, C. A., Heim, B., Dubinenkov, I, Kraberg, A., Moiseev, D., & Bracher, A. (2015). From fresh to marine waters: Characterization and fate of dissolved organic matter in the Lena River delta region, Siberia. *Frontiers in Marine Science*, *2*, 108. https://doi.org/10.3389/fmars.2015.00108

Guay, C. K., McLaughlin, F. A., & Yamamoto-Kawai, M. (2009). Differentiating fluvial components of Upper Canada Basin waters on the basis of measurements of dissolved barium combined with other physical and chemical tracers. *Journal of Geophysical Research*, *114*(C1), C00A09. https://doi.org/10.1029/2008jc005099

Guéguen, C., Itoh, M., Kikuchi, T., Eert, J., & Williams, W. J. (2015). Variability in dissolved organic matter optical properties in surface waters in the Amerasian Basin. *Frontiers in Marine Science*, *2*, 78. https://doi.org/10.3389/fmars.2015.00078

Haine, T. W. N., Curry, B., Gerdes, R., Hansen, E., Karcher, M., Lee, C., et al. (2015). Arctic freshwater export: Status, mechanisms, and prospects. *Global and Planetary Change*, *125*, 13–35. https://doi.org/10.1016/j.gloplacha.2014.11.013

Halewood, E., Opalk, K., Custals, L., Carey, M., Hansell, D. A., & Carlson, C. A. (2010). GO-SHIP Repeat Hydrography: Determination of dissolved organic carbon (DOC) and total dissolved nitrogen (TDN) in seawater using high temperature combustion analysis. In E. M. Hood, C. L. Sabine, & B. M. Sloyan (Eds.), *The GO-SHIP repeat hydrography manual: A collection of expert reports and guidelines*, *IOCCP report number 14*. ICPO Publication Series Number 134 Retrieved from http://www.go-ship.org/HydroMan.html

Hansell, D. A. (2005). Dissolved organic Carbon reference material program. *Eos, Transactions American Geophysical Union*, *86*(35), 318. https://doi.org/10.1029/2005EO350003

Hansell, D. A. (2017). *Arctic dissolved organic carbon (DOC) and total dissolved nitrogen (TDN) collected during POLARSTERN cruise PS94 (GEOTRACES) in 2015*. Rosenstiel School of Marine & Atmospheric Sciences, University of Miami. https://doi.org/10.1594/PANGAEA.884113

Hansell, D. A. (2021). DOC data from Cruise 33HQ20150809, exchange version. CCHDO cruise https://cchdo.ucsd.edu/cruise/33HQ20150809. Accessed from CCHDOAccess date 2021-03-27. https://doi.org/10.7942/C2MW25

Helms, J. R., Stubbins, A., Ritchie, J. D., Minor, E. C., Kieber, D. J., & Mopper, K. (2008). Absorption spectral slopes and slope ratios as indicators of molecular weight, source, and photobleaching of chromophoric dissolved organic matter. *Limnology & Oceanography*, *53*(3), 955–969. https://doi.org/10.4319/lo.2008.53.3.0955

Hölemann, J. A., Juhls, B., Bauch, D., Janout, M., Koch, B. P., & Heim, B. (2021). The impact of land-fast ice on the distribution of terrestrial dissolved organic matter in the Siberian Arctic shelf seas. *Biogeosciences Discussions*, 1–30.

Holmes, R. M., McClelland, J. W., Tank, S. E., Spencer, R. G. M., & Shiklomanov, A. I. (2019). *Arctic great rivers observatory*. ersion 20190904. Water Quality Dataset. Retrieved from https://arcticgreatrivers.org/data

Horner-Devine, A. R., Hetland, R. D., & MacDonald, D. G. (2015). Mixing and transport in coastal river plumes. *Annual Review of Fluid Mechanics*, *47*(1), 569–594. https://doi.org/10.1146/annurev-fluid-010313-141408

Jackson, J. M., Carmack, E. C., McLaughlin, F. A., Allen, S. E., & Ingram, R. G. (2010). Identification, characterization, and change of the near-surface temperature maximum in the Canada Basin, 1993-2008. *Journal of Geophysical Research*, *115*(C5), C05021. https://doi.org/10.1029/2009JC005265

Jakuba, R. W., Saito, M. A., Moffett, J. W., & Xu, Y. (2012). Dissolved zinc in the subArctic North Pacific and Bering Sea: Its distribution, speciation, and importance to primary producers. *Global Biogeochemical Cycles*, *26*(2), GB2015. https://doi.org/10.1029/2010GB004004

Jensen, L. T., Cullen, J. T., Jackson, S. L., Gerringa, L. J., Bauch, D., Middag, R., et al. (2022). A refinement of the processes controlling dissolved copper and nickel biochemistry: Insights from the pan-Arctic. *Journal of Geophysical Research: Oceans*, *127*(5), e2021jc018087. https://doi.org/10.1029/2021jc018087

Jensen, L. T., Morton, P., Twining, B. S., Heller, M. I., Hatta, M., Measures, C. I., et al. (2020). A comparison of marine Fe and Mn cycling: US GEOTRACES GN01 Western Arctic case study. *Geochimica et Cosmochimica Acta*, *288*, 138–160. https://doi.org/10.1016/j.gca.2020.08.006

Jensen, L. T., Wyatt, N. J., Twining, B. S., Rauschenberg, S., Landing, W. M., Sherrell, R. M., & Fitzsimmons, J. N. (2019). Biogeochemical cycling of dissolved Zinc in the Western Arctic (Arctic GEOTRACES GN01). *Global Biogeochemical Cycles*, *33*(3), 343–369. https://doi.org/10.1029/2018gb005975

Jiang, W., Gastineau, G., & Codron, F. (2021). Multicentennial variability driven by salinity exchanges between the Atlantic and the arctic ocean in a coupled climate model. *Journal of Advances in Modeling Earth Systems*, *13*(3), e2020MS002366. https://doi.org/10.1029/2020ms002366

Jones, E. P., & Anderson, L. G. (1986). On the origin of the chemical properties of the Arctic Ocean halocline. *Journal of Geophysical Research*, *91*(C9), 10759–10767. https://doi.org/10.1029/jc091ic09p10759

Jones, E. P., Anderson, L. G., Jutterström, S., Mintrop, L., & Swift, J. H. (2008). Pacific freshwater, river water and sea ice meltwater across Arctic Ocean basins: Results from the 2005 Beringia Expedition. *Journal of Geophysical Research*, *113*(C8), C08012. https://doi.org/10.1029/2007jc004124

Kadko, D., & Landing, W. (2015). U.S. Arctic GEOTRACES USCGC Healy (HLY1502) cruise report. Retrieved from https://www.bodc.ac.uk/resources/inventories/cruise_inventory/reports/healy1502.pdf

Kaiser, K., Benner, R., & Amon, R. M. W. (2017). The fate of terrigenous dissolved organic carbon on the Eurasian shelves and export to the North Atlantic. *Journal of Geophysical Research: Oceans*, *122*(1), 4–22. https://doi.org/10.1002/2016JC012380

Karcher, M., Smith, J. N., Kauker, F., Gerdes, R., & Smethie, W. M. (2012). Recent changes in Arctic Ocean circulation revealed by iodine-129 observations and modeling. *Journal of Geophysical Research*, *117*(C8). https://doi.org/10.1029/2011jc007513

Kikuchi, T., Hatakeyama, K., & Morison, J. H. (2004). Distribution of convective lower halocline water in the eastern Arctic Ocean. *Journal of Geophysical Research*, *109*(C12), C12030. https://doi.org/10.1029/2003JC002223

Klunder, M. B., Laan, P., Middag, R., De Baar, H. J. W., & Bakker, K. (2012). Dissolved iron in the Arctic Ocean: Important role of hydrothermal sources, shelf input and scavenging removal. *Journal of Geophysical Research*, *117*(C4). https://doi.org/10.1029/2011jc007135

Knust, R. (2017). Polar research and supply vessel POLARSTERN operated by the Alfred-Wegener-institute. *Journal of large-scale research facilities*, *3*, A119. https://doi.org/10.17815/jlsrf-3-163

Kondo, Y., Obata, H., Hioki, N., Ooki, A., Nishino, S., Kikuchi, T., & Kuma, K. (2016). Transport of trace metals (Mn, Fe, Ni, Zn and Cd) in the Western Arctic Ocean (Chukchi Sea and Canada basin) in late summer 2012. *Deep Sea Research Part I: Oceanographic Research Papers*, *116*, 236–252. https://doi.org/10.1016/j.dsr.2016.08.010

Korhonen, M., Rudels, B., Marnela, M., Wisotzki, A., & Zhao, J. (2013). Time and space variability of freshwater content, heat content and seasonal ice melt in the Arctic Ocean from 1991 to 2011. *Ocean Science*, *9*(6), 1015–1055. https://doi.org/10.5194/os-9-1015-2013

Kothawala, D. N., Stedmon, C. A., Müller, R. A., Weyhenmeyer, G. A., Köhler, S. J., & Tranvik, L. J. (2014). Controls of dissolved organic matter quality: Evidence from a large-scale boreal lake survey. *Global Change Biology*, *20*(4), 1101–1114. https://doi.org/10.1111/gcb.12488

Krachler, R., von der Kammer, F., Jirsa, F., Süphandag, A., Krachler, R. F., Plessl, C., et al. (2012). Nanoscale lignin particles as sources of dissolved iron to the ocean. *Global Biogeochemical Cycles*, *26*(3), 2012GB004294. https://doi.org/10.1029/2012gb004294

Krisch, S., Hopwood, M. J., Roig, S., Gerringa, L. J. A., Middag, R., Rutgers van der Loeff, M. M., et al. (2022). Arctic – Atlantic exchange of the dissolved micronutrients iron, manganese, cobalt, nickel, copper and zinc with a focus on Fram Strait. *Global Biogeochemical Cycles*, *36*(5), e2021GB007191. https://doi.org/10.1029/2021GB007191

Laglera, L. M., & van den Berg, C. M. (2003). Copper complexation by thiol compounds in estuarine waters. *Marine Chemistry*, *82*(1–2), 71–89. https://doi.org/10.1016/s0304-4203(03)00053-7

Laglera, L. M., & van den Berg, C. M. G. (2009). Evidence for geochemical control of iron by humic substances in seawater. *Limnology & Oceanography*, *54*(2), 610–619. https://doi.org/10.4319/lo.2009.54.2.0610

Laglera, L. M., Sukekava, C., Slagter, H. A., Downes, J., Aparicio-Gonzalez, A., Gerringa, L. J. A. (2019). First quantification of the controlling role of Humic substances in the transport of iron across the surface of the Arctic Ocean. *Environmental Science & Technology*.

Landing, W. M., Cutter, G., & Kadko, D. C. (2019). Bottle data from the GEOTRACES clean Carousel sampling system (GTC) on the Arctic section cruise (HLY1502) from August to October 2015 (U.S. GEOTRACES Arctic project). *Biological and Chemical Oceanography Data Management Office (BCO-DMO)*. https://doi.org/10.1575/1912/bco-dmo.647259.4

Landing, W. M., Cutter, G. A., & Kadko, D. C. (2017). CTD-ODF profiles from GEOTRACES-arctic section cruise HLY1502, August to October 2015 (U. S. GEOTRACES arctic project). Biological and chemical oceanography data management Office (BCO-dmo). (ersion 20160310CCHSIO-SEE) ersion Date 2017-05-22 [if applicable, indicate subset used]. Retrieved from http://lod.bco-dmo.org/id/dataset/700817

Li, H., Fedorov, A., & Liu, W. (2021). AMOC stability and diverging response to Arctic sea ice decline in two climate models. *Journal of Climate*, *34*(13), 5443–5460. https://doi.org/10.1175/jcli-d-20-0572.1

Maie, N., Pisani, O., & Jaffé, R. (2008). Mangrove tannins in aquatic ecosystems: Their fate and possible influence on dissolved organic carbon and nitrogen cycling. *Limnology & Oceanography*, *53*(1), 160–171. https://doi.org/10.4319/lo.2008.53.1.0160

Mathis, J. T., Pickart, R. S., Hansell, D. A., Kadko, D., & Bates, N. R. (2007). Eddy transport of organic carbon and nutrients from the Chukchi Shelf: Impact on the upper halocline of the western Arctic Ocean. *Journal of Geophysical Research*, *112*(C5), C05011. https://doi.org/10.1029/2006jc003899

McLaughlin, F. A., & Carmack, E. C. (2010). Deepening of the nutricline and chlorophyll maximum in the Canada Basin interior, 2003–2009. *Geophysical Research Letters*, *37*(24). https://doi.org/10.1029/2010gl045459

McLaughlin, F. A., Carmack, E. C., Carmack, R. W., Macdonald, H., Melling, J. H., Swift, P. A., et al. (2004). The joint roles of Pacific and Atlantic-origin waters in the Canada Basin, 1997–1998. *Deep-Sea Research, Part A: Oceanographic Research Papers I*, *51*, 107–128. https://doi.org/10.1016/j.dsr.20009.010

Metzner, E. P., Salzmann, M., & Gerdes, R. (2020). Arctic Ocean surface energy flux and the cold halocline in future climate projections. *Journal of Geophysical Research: Oceans*, *125*(2), e2019JC015554. https://doi.org/10.1029/2019jc015554

Middag, R., de Baar, H. J. W., Laan, P., & Klunder, M. B. (2011). Fluvial and hydrothermal input of manganese into the Arctic Ocean. *Geochimica et Cosmochimica Acta*, *75*(9), 2393–2408. https://doi.org/10.1016/j.gca.2011.02.011

Morel, F. M., & Price, N. M. (2003). The biogeochemical cycles of trace metals in the oceans. *Science*, *300*(5621), 944–947. https://doi.org/10.1126/science.1083545

Morison, J., Kwok, R., Dickinson, S., Andersen, R., Peralta-Ferriz, C., Morison, D., et al. (2021). The cyclonic mode of Arctic Ocean circulation. *Journal of Physical Oceanography*, *51*(4), 1053–1075. https://doi.org/10.1175/jpo-d-20-0190.1

Muller, F. L., & Batchelli, S. (2013). Copper binding by terrestrial versus marine organic ligands in the coastal plume of River Thurso, North Scotland. Estuarine. *Coastal and Shelf Science*, *133*, 137–146. https://doi.org/10.1016/j.ecss.2013.08.024

Murphy, K. R., Stedmon, C. A., Graeber, D., & Bro, R. (2013). Fluorescence spectroscopy and multi-way techniques. *PARAFAC Analytical Methods*, *5*(23), 6557. https://doi.org/10.1039/c3ay41160e

Murphy, K. R., Stedmon, C. A., Wenig, P., & Bro, R. (2014). OpenFluor–an online spectral library of auto-fluorescence by organic compounds in the environment. *Analytical Methods*, *6*(3), 658–661. https://doi.org/10.1039/c3ay41935e

Nakayama, Y., Fujita, S., Kuma, K., & Shimada, K. (2011). Iron and humic-type fluorescent dissolved organic matter in the Chukchi Sea and Canada Basin of the Western Arctic Ocean. *Journal of Geophysical Research*, *116*(C7), 2010JC006779. https://doi.org/10.1029/2010jc006779

Newton, R., Schlosser, P., Mortlock, R., Swift, J., & MacDonald, R. (2013). Canadian basin freshwater sources and changes: Results from the 2005 Arctic Ocean section. *Journal of Geophysical Research: Oceans*, *118*(4), 2133–2154. https://doi.org/10.1002/jgrc.20101

Nishimura, S., Kuma, K., Ishikawa, S., Omata, A., & Saitoh, S. I. (2012). Iron, nutrients, and humic-type fluorescent dissolved organic matter in the northern Bering Sea shelf, Bering Strait, and Chukchi Sea. *Journal of Geophysical Research*, *117*(C2). https://doi.org/10.1029/2011jc007355

Nixon, R. L., Jackson, S. L., Cullen, J. T., & Ross, A. R. (2019). Distribution of copper-complexing ligands in Canadian Arctic waters as determined by immobilized copper (II)-ion affinity chromatography. *Marine Chemistry*, *215*, 10367. https://doi.org/10.1016/j.marchem.2019.103673

Oldham, V. E., Lamborg, C. H., & Hansel, C. M. (2020). The spatial and temporal variability of Mn speciation in the coastal northwest Atlantic Ocean. *Journal of Geophysical Research: Oceans*, *125*(1), e2019JC015167. https://doi.org/10.1029/2019jc015167

Oldham, V. E., Mucci, A., Tebo, B. M., & Luther, G. W., III. (2017). Soluble Mn (III)–L complexes are abundant in oxygenated waters and stabilized by humic ligands. *Geochimica et Cosmochimica Acta*, *199*, 238–246. https://doi.org/10.1016/j.gca.2016.11.043

Opsahl, S., & Benner, R. (1997). Distribution and cycling of terrigenous dissolved organic matter in the ocean. *Nature*, *386*(6624), 480–482. https://doi.org/10.1038/386480a0

Opsahl, S., Benner, R., & Amon, R. M. W. (1999). Major flux of terrigenous dissolved organic matter through the Arctic Ocean. *Limnology & Oceanography*, *44*(8), 2017–2023. https://doi.org/10.4319/lo.1999.44.8.2017

Paffrath, R., Laukert, G., Bauch, D., van der Loeff, M. R., & Pahnke, K. (2021). Separating individual contributions of major Siberian Rivers in the transpolar Drift of the Arctic Ocean. *Scientific Reports*, *11*(1), 1–11. https://doi.org/10.1038/s41598-021-86948-y

Paqualini, A. (2021). *Circulation pathways, time scales, and water mass composition in the Arctic Ocean: Results from 25 years of tracer observations*. Dissertation, Columbia University Libraries. https://doi.org/10.7916/d8-8a0m-9n67

Pasqualini, A., Schlosser, P., Newton, R., & Koffman, T. N. (2017). U.S. GEOTRACES Arctic section ocean water hydrogen and oxygen stable isotope analyses (version 1.0) [dataset]. Interdisciplinary Earth Data Alliance (IEDA). https://doi.org/10.1594/ieda/100633

Pokrovsky, O. S., Viers, J., Dupre, B., Chabaux, F., Gaillardet, J., Audry, S., et al. (2012). Biogeochemistry of carbon, major and trace elements in watersheds of northern Eurasia drained to the Arctic Ocean: The change of fluxes, sources and mechanisms under the climate warming prospective. *Comptes Rendus Geoscience*, *344*(11–12), 663–677. https://doi.org/10.1016/j.crte.2012.08.003

Polyakov, I. V., Bhatt, U. S., Walsh, J. E., Abrahamsen, E. P., Pnyushkov, A. V., & Wassmann, P. F. (2013). Recent oceanic changes in the Arctic in the context of long-term observations. *Ecological Applications*, *23*(8), 1745–1764. https://doi.org/10.1890/11-0902.1

Proshutinsky, A., Krishfield, R., & Timmermans, M. L. (2020). Introduction to special collection on Arctic Ocean modeling and observational synthesis (FAMOS) 2: Beaufort Gyre phenomenon. *Journal of Geophysical Research: Oceans*, *125*(2), e2019JC015400. https://doi.org/10.1029/2019jc015400

Proshutinsky, A., Krishfield, R., Toole, J. M., Timmermans, M. L., Williams, W., Zimmermann, S., et al. (2019). Analysis of the Beaufort gyre freshwater content in 2003–2018. *Journal of Geophysical Research: Oceans*, *124*(12), 9658–9689. https://doi.org/10.1029/2019jc015281

Proshutinsky, A. Y., & Johnson, M. A. (1997). Two circulation regimes of the wind-driven Arctic Ocean. *Journal of Geophysical Research*, *102*(C6), 12493–12514. https://doi.org/10.1029/97jc00738

Rabe, B., Karcher, M., Kauker, F., Schauer, U., Toole, J. M., Krishfield, R. A., et al. (2014). Arctic Ocean liquid freshwater storage trend 1992-2012. *Geophysical Research Letters*, *41*(3), 961–968. https://doi.org/10.1002/2013GL058121

Rabe, B., Schauer, U., Ober, S., Horn, M., Hoppmann, M., Korhonen, M., et al. (2016a). Physical oceanography during POLARSTERN cruise PS94 (ARK-XXIX/3). *Alfred Wegener Institute, Helmholtz Centre for Polar and Marine Research, Bremerhaven, PANGAEA*. https://doi.org/10.1594/PANGAEA.859558

Rabe, B., Schauer, U., Ober, S., Horn, M., Hoppmann, M., Korhonen, M., et al. (2016b). Physical oceanography measured on water bottle samples during POLARSTERN cruise PS94 (ARK-XXIX/3). *Alfred Wegener Institute, Helmholtz Centre for Polar and Marine Research, Bremerhaven, PANGAEA*. https://doi.org/10.1594/PANGAEA.859559

Raspor, B., Nürnberg, H. W., Valenta, P., & Branica, M. (1984). Studies in seawater and lake water on interactions of trace metals with humic substances isolated from marine and estuarine sediments: II. Voltammetric investigations on trace metal complex formation in the dissolved phase. *Marine Chemistry*, *15*(3), 231–249. https://doi.org/10.1016/0304-4203(84)90020-3

Rennermalm, A. K., Wood, E. F., Déry, S. J., Weaver, A. J., & Eby, M. (2006). Sensitivity of the thermohaline circulation to Arctic Ocean runoff. *Geophysical Research Letters*, *33*(12), L12703. https://doi.org/10.1029/2006gl026124

Rijkenberg, M. J. A., Slagter, H. A., Rutgers van der Loeff, M. M., van Ooijen, J. C., & Gerringa, L. J. A. (2018). Dissolved Fe in the deep and upper Arctic Ocean with a focus on Fe limitation in the Nansen Basin. *Frontiers in Marine Science*, *5*. https://doi.org/10.3389/fmars.2018.00088

Rudels, B. (2001). Ocean current: Arctic basin circulation. In J. Steele, S. Thorpe, & K. Turekian (Eds.), *Encyclopedia of Ocean Sciences* (pp. 177–187).

Rudels, B. (2009). *Arctic Ocean circulation*. Academic Press.

Rudels, B. (2015). Arctic Ocean circulation, processes and water masses: A description of observations and ideas with focus on the period prior to the international polar year 2007–2009. *Progress in Oceanography*, *132*, 22–67. https://doi.org/10.1016/j.pocean.2013.11.006

Rudels, B., Anderson, L. G., & Jones, E. P. (1996). Formation and evolution of the surface mixed layer and halocline of the Arctic Ocean. *Journal of Geophysical Research*, *101*(C4), 8807–8821. https://doi.org/10.1029/96jc00143

Sakshaug, E. (2004). *Primary and secondary production in the Arctic seas, the organic carbon cycle in the Arctic Ocean* (pp. 57–81). Springer.

Schauer, U. (2016). The expedition PS94 of the research vessel POLARSTERN to the central Arctic Ocean in 2015, Bremerhaven, Alfred wegener Institute for polar and marine research. *Berichte zur Polar- und Meeresforschung = Reports on polar and marine research 703 170 pp.*

Schlitzer, R. (2020). Ocean Data View. ODV 5.2. 1.

Schlosser, P., Bauch, D., Fairbanks, R., & Bönisch, G. (1994). Arctic river-runoff: Mean Residence time on the shelves and in the halocline. *Deep Sea Research Part I: Oceanographic Research Papers*, *41*(7), 1053–1068. https://doi.org/10.1016/0967-0637(94)90018-3

Semeniuk, D. M., Bundy, R. M., Payne, C. D., Barbeau, K. A., & Maldonado, M. T. (2015). Acquisition of organically complexed copper by marine phytoplankton and bacteria in the northeast subarctic Pacific ocean. *Marine Chemistry*, *173*, 222–223. https://doi.org/10.1016/j.marchem.2015.01.005

Shank, G. C., Skrabal, S. A., Whitehead, R. F., & Kieber, R. J. (2004). Strong copper complexation in an organic-rich estuary: The importance of allochthonous dissolved organic matter. *Marine Chemistry*, *88*(1–2), 21–39. https://doi.org/10.1016/j.marchem.2004.03.001

Shen, Y., Benner, R., Robbins, L. L., & Wynn, J. G. (2016). Sources, distributions, and dynamics of dissolved organic matter in the Canada and Makarov Basins. *Frontiers in Marine Science*, *3*, 198. https://doi.org/10.3389/fmars.2016.00198

Shimada, K., Carmack, E. C., Hatakeyama, K., & Takizawa, T. (2001). Varieties of shallow temperature maximum waters in the Western Canadian Basin of the Arctic Ocean. *Geophysical Research Letters*, *28*(18), 3441–3444. https://doi.org/10.1029/2001gl013168

Sholkovitz, E. R., & Copland, D. (1981). The coagulation, solubility and adsorption properties of Fe, Mn, Cu, Ni, Cd, Co and humic acids in a river water. *Geochimica et Cosmochimica Acta*, *45*(2), 181–189. https://doi.org/10.1016/0016-7037(81)90161-7

Slagter, H. A., Laglera, L. M., Sukekava, C., & Gerringa, L. J. A. (2019). Fe-binding organic ligands in the humic-rich TransPolarDrift in the surface Arctic Ocean using multiple voltammetric methods. *Journal of Geophysical Research: Ocean*, *124*(3), 1491–1508. https://doi.org/10.1029/2018jc014576

Slagter, H. A., Reader, H. E., Rijkenberg, M. J. A., Van Der Loeff, M. R., de Baar, H. J. W., & Gerringa, L. J. A. (2017). Organic Fe speciation in the Eurasian basins of the Arctic Ocean and its relation to terrestrial DOM. *Marine Chemistry*, *197*, 11–25. https://doi.org/10.1016/j.marchem.2017.10.005

Sohn, M. L., & Hughes, M. C. (1981). Metal ion complex formation constants of some sedimentary humic acids with Zn (II), Cu (II) and Cd (II). *Geochimica et Cosmochimica Acta*, *45*(12), 2393–2399. https://doi.org/10.1016/0016-7037(81)90093-4

Stedmon, C. A., Amon, R. M. W., Bauch, D., Bracher, A., Gonçalves-Araujo, R., Hoppmann, M., et al. (2021). Insights into water mass origins in the central Arctic Ocean from in-situ dissolved organic matter fluorescence. *Journal of Geophysical Research: Oceans*, *126*(7), e2021JC017407. https://doi.org/10.1029/2021JC017407

Stedmon, C. A., Amon, R. M. W., Rinehart, A. J., & Walker, S. A. (2011). The supply and characteristics of colored dissolved organic matter (CDOM) in the Arctic Ocean: Pan Arctic trends and differences. *Marine Chemistry*, *124*(1–4), 108–118. https://doi.org/10.1016/J.MARCHEM.2010.12.007

Stedmon, C. A., Thomas, D. N., Papadimitriou, S., Granskog, M. A., & Dieckmann, G. S. (2011). Using fluorescence to characterize dissolved organic matter in Antarctic sea ice brines. *Journal of Geophysical Research*, *116*(G3), G03027. https://doi.org/10.1029/2011jg001716

Sunda, W. G. (2012). Feedback interactions between trace metal nutrients and phytoplankton in the ocean. *Frontiers in Microbiology*, *3*, 204. https://doi.org/10.3389/fmicb.2012.00204

Thibodeau, B., & Bauch, D. (2015). River water and brine inventory over the Laptev Sea shelf: 2007 to 2011. In *AGU fall meeting abstracts* (Vol. *2014*, pp. OS51C–1005).

Thibodeau, B., Bauch, D., Kassens, H., & Timokhov, L. A. (2014). Interannual variations in river water content and distribution over the Laptev Sea between 2007 and 2011: The Arctic dipole connection. *Geophysical Research Letters*, *41*(20), 7237–7244. https://doi.org/10.1002/2014gl061814

Ulfsbo, A., Jones, E. M., Casacuberta, N., Korhonen, M., Rabe, B., Karcher, M., & Van Heuven, S. M. (2018). Rapid changes in anthropogenic carbon storage and ocean acidification in the intermediate layers of the Eurasian Arctic Ocean: 1996–2015. *Global Biogeochemical Cycles*, *32*(9), 1254–1275. https://doi.org/10.1029/2017gb005738

Van den Berg, C. M. G., & Nimmo, M. (1987). Determination of interactions of nickel with dissolved organic material in seawater using cathodic stripping voltammetry. *Science of the Total Environment*, *60*, 185–195. https://doi.org/10.1016/0048-9697(87)90415-3

Vraspir, J. M., & Butler, A. (2009). Chemistry of marine ligands and siderophores.

Walker, S. A., Amon, R. M. W., Stedmon, C., Duan, S. W., & Louchouarn, P. (2009). The use of PARAFAC modeling to trace terrestrial dissolved organic matter and fingerprint water masses in coastal Canadian Arctic surface waters. *Journal of Geophysical Research*, *114*, G00F06. https://doi.org/10.1029/2009jg000990

Walker, S. A., Amon, R. M. W., & Stedmon, C. A. (2013). Variations in high-latitude riverine fluorescent dissolved organic matter: A comparison of large Arctic rivers. *Journal of Geophysical Research: Biogeosciences*, *118*(4), 1689–1702. https://doi.org/10.1002/2013jg002320

Wang, D., Henrichs, S. M., & Guo, L. (2006). Distributions of Nutrients, dissolved organic carbon and carbohydrates in the Western Arctic Ocean. *Continental Shelf Research*, *26*(14), 1654–1667. https://doi.org/10.1016/j.csr.2006.05.001

Watanabe, E. (2013). Linkages among halocline variability, shelf-basin interaction, and wind regimes in the Beaufort Sea demonstrated in pan-Arctic ocean modeling framework. *Ocean Modelling*, *71*, 43–45. https://doi.org/10.1016/j.ocemod.2012.12.010

Whitmore, L. M., Pasqualini, A., Newton, R., & Shiller, A. M. (2020). Gallium: A new tracer of Pacific water in the Arctic Ocean. *Journal of Geophysical Research: Oceans*, *125*(7), e2019JC015842. https://doi.org/10.1029/2019jc015842

Williford, T., Amon, R. M. W., Benner, R., Kaiser, K., Bauch, D., Stedmon, C., et al. (2021). Insights into the origins, molecular characteristics and distribution of iron-binding ligands in the Arctic Ocean. *Marine Chemistry*, *231*, 103936. https://doi.org/10.1016/j.marchem.2021.103936

Woodgate, R. A., Weingartner, T. J., & Lindsay, R. (2012). Observed increases in Bering Strait oceanic fluxes from the Pacific to the Arctic from 2001 to 2011 and their impacts on the Arctic Ocean water column. *Geophysical Research Letters*, *39*(24), 2012GL054092. https://doi.org/10.1029/2012gl054092

Woosley, R. J., Millero, F. J., & Takahashi, T. (2017). Internal consistency of the inorganic carbon system in the Arctic Ocean. *Limnology and Oceanography: Methods*, *15*(10), 887–896. https://doi.org/10.1002/lom10208

Yamamoto-Kawai, M., McLaughlin, F. A., Carmack, E. C., Nishino, S., & Shimada, K. (2008). Freshwater budget of the Canada basin, Arctic Ocean, from salinity, δ18O, and nutrients. *Journal of Geophysical Research*, *113*(C1), C01007. https://doi.org/10.1029/2006jc003858

Yamamoto-Kawai, M., McLaughlin, F. A., Carmack, E. C., Nishino, S., Shimada, K., & Kurita, N. (2009). Surface freshening of the Canada Basin, 2003–2007: River runoff versus sea ice meltwater. *Journal of Geophysical Research*, *114*(C1), C00A05. https://doi.org/10.1029/2008jc005000

Yamashita, Y., Boyer, J. N., & Jaffé, R. (2013). Evaluating the distribution of terrestrial dissolved organic matter in a complex coastal ecosystem using fluorescence spectroscopy. *Continental Shelf Research*, *66*, 136–144. https://doi.org/10.1016/j.csr.2013.06.010

Yan, G., & Kaiser, K. (2018a). A rapid and sensitive method for the analysis of lignin phenols in environmental samples using ultra-high performance liquid chromatography-electrospray ionization-tandem mass spectrometry with multiple reaction monitoring. *Analytica Chimica Acta*, *1023*, 74–80. https://doi.org/10.1016/j.aca.2018.03.054

Yan, G., & Kaiser, K. (2018b). Ultra-low sample volume cupric sulfate oxidation method for the analysis of dissolved lignin. *Analytical Chemistry*, *68*(1–2), 59–70. https://doi.org/10.1021/acs.analchem.8b01867

Zhang, P., Wu, Z., & Jin, R. (2021). How can the winter North Atlantic Oscillation influence the early summer precipitation in Northeast Asia: Effect of the Arctic sea ice. *Climate Dynamics*, *56*(5), 1989–2005. https://doi.org/10.1007/s00382-020-05570-2

Zhang, R., Jensen, L. T., Fitzsimmons, J. N., Sherrell, R. M., & John, S. (2019). Dissolved cadmium and cadmium stable isotopes in the Western Arctic ocean. *Geochimica et Cosmochimica Acta*, *258*, 258–273. https://doi.org/10.1016/j.gca.2019.05.028

Zhang, Y., Yamamoto-Kawai, M., & Williams, W. J. (2020). Two decades of ocean acidification in the surface waters of the Beaufort Gyre, Arctic Ocean: Effects of sea ice melt and retreat from 1997–2016. *Geophysical Research Letters*, *47*(3), e60119. https://doi.org/10.1029/2019gl086421

Zhengbin, Z., & Liansheng, L. (1982). Microcosmic approach to marine chemistry—A Φ (Z/l, *x*) rule of chemical processes in seawater and its applications. *Chinese Journal of Oceanology and Limnology*, *1*(1), 54–75. https://doi.org/10.1007/bf02852890

Zhong, W., & Zhao, J. (2014). Deepening of the Atlantic water core in the Canada Basin in 2003–11. *Journal of Physical Oceanography*, *44*(9), 2353–2369. https://doi.org/10.1175/jpo-d-13-084.1

References From the Supporting Information

Gonçalves-Araujo, R., Stedmon, C. A., de Steur, L., Osburn, C. L., & Granskog, M. A. (2020). A decade of annual Arctic DOC export with polar surface water in the east Greenland current. *Geophysical Research Letters*, *47*(20), e2020GL089686. https://doi.org/10.1029/2020gl089686